Journal of Materials Chemistry B

ROYAL SOCIETY OF CHEMISTRY

PAPER

View Article Online
View Journal | View Issue

Cite this: J. Mater. Chem. B, 2025, 13, 10552

Cross-linked poly(alkylene citrates) with L-glutathione for vascular tissue engineering: structure–property relationships and cell-type dependent response to oxidative stress†

Filip Koper,[a] Dominika Grzywna,[a] Lucie Svobodová,[b] Antonín Sedlář,[b] Libor Kobera,[c] Tomáš Riedel,[d] Zuzana Riedelová,[d] Agata Flis,[e] Hynek Beneš,[f] Elżbieta Pamuła,[e] Lucie Bačáková *[b] and Wiktor P. Kasprzyk *[a]

Cross-linked poly(alkylene citates) (cPAC) based on 1,6-hexanediol (cPHC) and 1,8-octanediol (cPOC) and modified with 0.4, 0.8 and 1.6% w/w L-glutathione (GSH) were synthesized as potential materials for vascular tissue engineering. The materials prepared at a citric acid : diol molar ratio of 2 : 3 exhibited superior mechanical strength and reduced acidity in comparison to the 1 : 1 materials. All materials exhibited blue fluorescence, which intensity was enhanced with increasing GSH concentration. Conversely, the latter demonstrated marginally enhanced antioxidant properties. The preliminary cell culture tests of the 2 : 3 materials with human adipose tissue stem cells (ASCs) revealed that cPOC did not provide an appropriate environment for cell colonization due to its higher acidity than cPHC. In contrast, cPHC promoted the growth of ASCs and other cell types, including fibroblasts (NHDFs), endothelial cells (HUVECs), and smooth muscle cells (SMCs), at all GSH concentrations, with minimal negative effect on HUVEC and SMC proliferation. The induction of oxidative stress by menadione demonstrated a notable decline in the metabolic activity of both ASCs and NHDFs on cPHCs across all GSH concentrations. However, an incremental protective effect on the cells was observed with increasing GSH concentrations. In contrast, HUVECs and SMCs demonstrated increased metabolic activity, without the protective effect of GSH being observed. Therefore, the findings demonstrate that cell type-specific differences exist in cell response to oxidative stress. Consequently, the addition of antioxidants to the polymer should be guided by the intended cell type for use in vascular reconstruction. Our results also suggest an intrinsic antioxidant activity of cPHC materials and their good hemocompatibility with human blood *in vitro*.

Received 15th November 2024,
Accepted 24th May 2025

DOI: 10.1039/d4tb02563f

rsc.li/materials-b

1. Introduction

Cardiovascular diseases continue to represent a significant global public health concern, particularly in light of their high mortality rates and often delayed detection.[1–3] A variety of pharmacological and preventive measures are employed in the medical treatment of cardiovascular conditions. However, surgical intervention is frequently the sole recourse for salvaging the patient.[1,4,5] In surgical treatment, autogenous grafts of the patient's healthy vessels are typically employed for the replacement of diseased or damaged structures.[6] Nevertheless, the condition of the vessels on occasion precludes their use, thereby necessitating the utilization of synthetic equivalents.[7] In vascular tissue engineering, a variety of materials are employed, including purely synthetic materials, materials of natural origin, and various composites combining synthetic

[a] Cracow University of Technology, Faculty of Chemical Engineering and Technology, Department of Biotechnology and Physical Chemistry, 24 Warszawska Str., 31-155 Krakow, Poland. E-mail: wiktor.kasprzyk@pk.edu.pl
[b] Czech Academy of Sciences, Institute of Physiology, Department of Biomaterials and Tissue Engineering, 1083 Vídeňská Str., 142 20 Prague, Czech Republic. E-mail: Lucie.Bacakova@fgu.cas.cz
[c] Czech Academy of Sciences, Institute of Macromolecular Chemistry, Department of Structural Analysis, Heyrovského nám. 1888/2, 162 00 Prague, Czech Republic
[d] Czech Academy of Sciences, Institute of Macromolecular Chemistry, Department of Chemistry and Physics of Surfaces and Biointerfaces, Heyrovského nám. 1888/2, 162 00 Prague, Czech Republic
[e] AGH University of Krakow, Faculty of Materials Science and Ceramics, Department of Biomaterials and Composites, 30 Adam Mickiewicza Ave., 30-059 Krakow, Poland
[f] Czech Academy of Sciences, Institute of Macromolecular Chemistry, Department of Polymer Processing, Heyrovského nám. 1888/2, 162 00 Prague, Czech Republic

† Electronic supplementary information (ESI) available. See DOI: https://doi.org/10.1039/d4tb02563f

structures with those of biological origin.[8–10] It is imperative that emerging materials meet a number of rigorous criteria in order to be suitable for particular applications. These include high biocompatibility, suitable mechanical and surface properties that can be modified, and, in the case of vascular scaffolds, low thrombogenicity.[8,11–14] The fundamental challenge in tissue engineering is to identify a material that meets the requisite specifications for a given application while maintaining a cost-effective manufacturing process and versatility in application. The currently available materials, including ePTFE, PCL, PGA, PET, PLLA, collagen, and elastin, have inherent limitations. Synthetic materials frequently elicit an immune response, thrombogenicity, and cellular oxidative stress, necessitating the application of coating materials that enhance their biological characteristics.[15,16] In contrast, natural materials retain full biocompatibility; however, their mechanical properties and strength severely limit their applicability.[17–19] Furthermore, the aforementioned synthetic materials are predominantly employed for the replacement of large-diameter vessels, which are typically acellular. In large-diameter vessels, relatively strong blood flow prevents the adhesion of undesirable cell types, including platelets, immune system cells, and smooth muscle cell precursors which can lead to stenosis of the graft. Modern small-diameter vascular grafts, however, necessitate the reconstruction of the physiological layers of the vascular wall, at the very least the inner layer of the endothelium, which is the most effective anti-thrombotic agent, and ideally also the tunica media with smooth muscle cells that provide contractile function. Therefore, the unfavorable biocompatibility and hemocompatibility characteristics of the currently used materials play an even greater role in small-diameter vascular tissue engineering, effectively hindering the application of these materials.[20,21]

Cross-linked poly(alkylene citrates) (cPACs) appear to be a promising class of polymers with the attributes of a versatile material for tissue engineering applications.[22–24] The biocompatible monomers utilized in their fabrication and the extensive range of mechanical properties modifications allow for the combination of the strength and durability of synthetic materials with the biocompatibility of materials of natural origin. Numerous *in vitro* studies have documented the biocompatibility and hemocompatibility of cPACs. cPACs possess extensive structural modification capabilities, allowing the imparting of new functionalities[25–27] and they are still under development for further functionalization.[28–33] However, apart from our previous work,[24,28] the extant literature discloses only a limited number of studies on cPACs and analogous materials for vascular tissue engineering. A PVA-citric acid polyester with potential application as a scaffold for vascular tissue engineering was reported.[34] In recent years, citrate-based materials have emerged as a viable option for the fabrication of 3D printable vascular scaffolds. For instance, a 3D-printed radio-opaque vascular scaffold has been developed based on methacrylated poly(1,12-dodecamethylene citrate) and molybdenum disulfide nanosheets,[35] additionally, highly elastic, 3D printable, and biodegradable citrate rubber *i.e.*, poly(tetrahydrofuran-*co*-citrate-*co*-hydroxytelechelic natural rubber) has demonstrated promise in its application as a vascular scaffold, as evidenced by its use in research studies.[36] Furthermore, an injectable citrate-containing polyester hydrogel for cardiac repair following myocardial infarction has been demonstrated to significantly reduce infarct size and scar formation while promoting neovascularization.[37]

In our research to date, we have concentrated on a comprehensive revision of the synthesis protocol and a detailed examination of the physicochemical and structural properties of PAC-based materials.[24] Nevertheless, a substantial quantity of research is currently being conducted on cPACs with the objective of introducing new functionalities into the structure of the materials through the use of small molecule modifiers.[38–41] Existing literature reports demonstrated a beneficial outcome provided by the introduction of modifications to the materials, among which fluorescence and antioxidant properties emerged as the most promising. Biodegradable photoluminescent polymers (BPLPs), based on the implementation of L-cysteine to cPACs, have been effectively applied to precise *in vivo* scaffold degradation control by fluorescence imaging.[42,43] Antioxidant cPACs produced *via* incorporation of ascorbic acid showed the potential to reduce inflammatory effects by quenching reactive oxygen species (ROS).[44] However, existing work describes attempts to modify cPAC materials with modifiers that are responsible for imparting a single new functionality to the material during the modification protocol.[38,44] It was therefore decided to carry out the modifications in such a way as to introduce both new properties into the final PAC materials using a single modifier. The overall goal was to confirm the suitability of the resulting materials for use in vascular tissue engineering through cytocompatibility studies and *in vitro* antioxidant properties.

2. Results and discussion

Cross-linked poly(alkylene citrate) (cPAC) control materials were obtained *via* the polycondensation reaction described in a previous study (Fig. 1).[24] GSH-modified cPAC materials (G_cPACs) were fabricated in an identical manner, except that a modifier-doped prepolymer solution was used for the cross-linking reaction.

The reaction of citric acid (CA) with 1,6-hexanediol or 1,8-octanediol at two molar ratios—1 : 1 and 2 : 3 (CA : diol)—led to the formulation of poly(hexamethylene citrate) (PHC_1 : 1 and PHC_2 : 3) and poly(octamethylene citrate) (POC_1 : 1 and POC_2 : 3) prepolymers, as well as the corresponding cross-linked materials (cPHC_1 : 1, cPHC_2 : 3, cPOC_1 : 1, and cPOC_2 : 3), obtained after 4 or 10 days of crosslinking (indicated by the appropriate suffix throughout the paper, *i.e.*, 4d or 10d, respectively).

Modification was performed using L-glutathione (GSH) solutions of varying concentrations, resulting in materials with final GSH contents of 0.4%, 0.8%, and 1.6% v/v, denoted by the suffixes G0.4, G0.8, and G1.6, respectively. The properties of the obtained materials discussed herein are strictly dependent on both the modification protocol and the synthesis–structure relationships described in our previous study.[24] Material characterization was

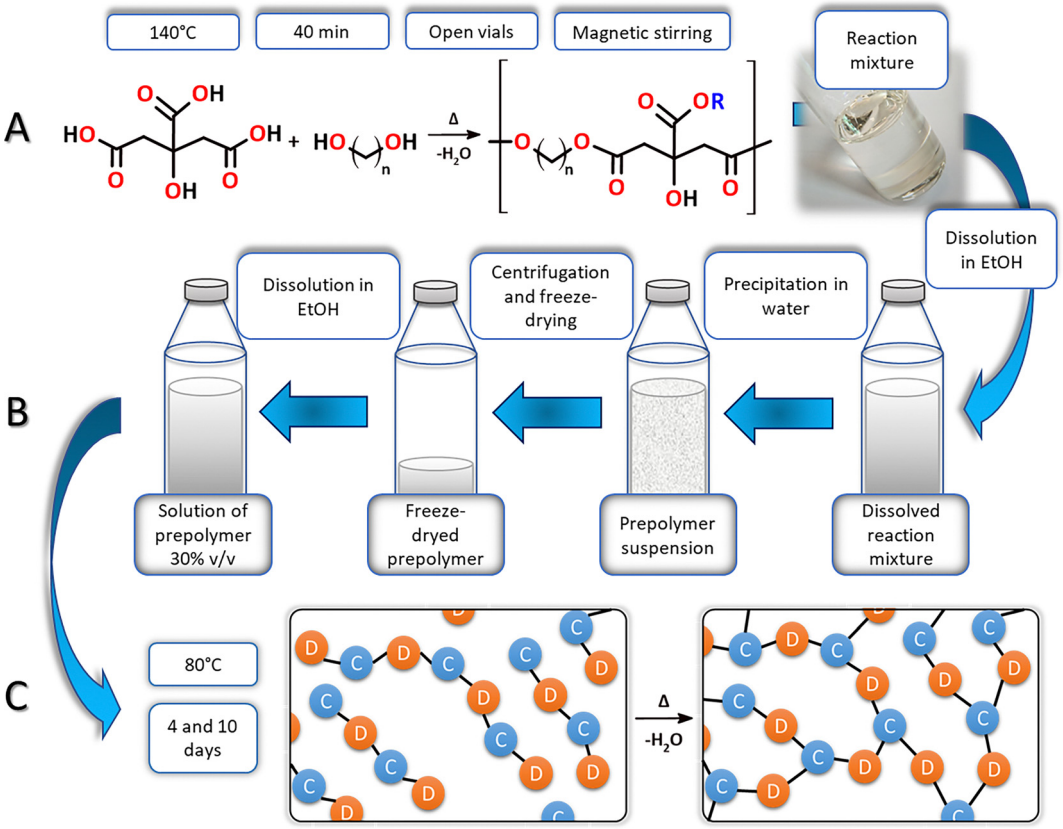

Fig. 1 The overall route for cPAC materials fabrication: prepolymer synthesis *via* polycondensation of CA and selected diols leading to a predominantly linear oligomer formation (A), multistep purification procedure (B), cross-linking reaction – bond formation mainly between α-carboxyl group from citrate residues and hydroxyl groups from hexa – or octamethylene chains (C).[24]

carried out using ^{13}C MAS NMR spectroscopy, fluorescence measurements, and antioxidant activity assays. The effects of GSH modification were further evaluated through dynamic mechanical analysis (DMA), thermal analysis (TGA/DSC), and comprehensive biological studies, including assessment of material biocompatibility with cells *in vitro*.

For biological experiments, materials modified with three GSH concentrations (0.4%, 0.8%, and 1.6% v/v) and unmodified control samples were used. Therefore, the influence of GSH incorporation on the properties of cPACs could be systematically elucidated.

2.1. Synthesis, modification and characterization of G_cPACs

2.1.1. Synthesis of G_cPAC materials. For the preparation of GSH-modified polymers (G_cPACs), aqueous GSH solutions prepared as described below were used. Appropriate amounts of each GSH solution were added to pure ethanolic solutions of prepolymers, which were then subjected to the crosslinking process (Fig. 18 in the Experimental section). A series of modified materials was thus obtained, as detailed in Table 3 (Experimental section). The resulting materials, similar to the control PAC samples, were transparent elastomers with smooth surfaces, distinguished only by an orange coloration that intensified with increasing GSH content (Fig. 2B). This coloration may result from low-molecular-weight substances formed *via* reactions between thermally induced GSH hydrolysis products, most notably L-cysteine (CYS). Under crosslinking conditions, CYS is prone to react with residual CA groups, forming ring-fused 2-pyridone analogs, which have been associated with strong yellow-orange coloration.[45,46] Moreover, as described below, the GSH-derived fluorescent compound formed *in situ* during crosslinking also exhibits a yellow hue in its pure form, potentially contributing to the observed coloration of the materials.

As stated previously in the Introduction, the choice of modifier was driven by the need to introduce both fluorescence and antioxidant properties through a single operational step. It was hypothesized that GSH would serve as an appropriate modifying agent due to its structure and properties, enabling bifunctional incorporation into the material network (Fig. 2A). The cysteinyl residues in the GSH structure are capable of reacting with CA following the thermally induced hydrolysis of GSH into a dipeptide, leading to the formation of 2-pyridone analogs.[47] Thus, the addition of GSH to the prepolymer prior to crosslinking was expected to result in the *in situ* formation of fluorescent derivatives within the material network. The potential antioxidant properties were attributed to both the physical entrapment and covalent incorporation of GSH molecules, as well as residual dipeptides and cysteine moieties formed during thermal hydrolysis. Their presence was anticipated to endow the materials with the ability to quench reactive oxygen

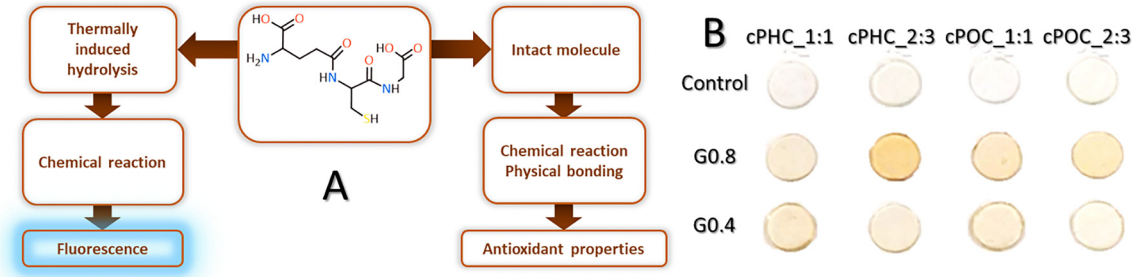

Fig. 2 The dual modification scheme of G_cPACs (A) and photograph of the obtained materials (B).

species (ROS) over an extended period through the gradual release of GSH as scaffold degradation progresses.

To verify this hypothesis, comprehensive material characterization was performed, and the results are presented in the subsequent sections.

2.1.2. Materials characterization

2.1.2.1. Structural characterization. The modified cPAC materials exhibited properties comparable to those of their control counterparts in numerous aspects. Consequently, the characterization methods employed in the following sections are, for the most part, identical to those used in our previous studies.[24,48] However, due to the modifications aimed at imparting fluorescent and antioxidant properties, additional investigations were conducted to validate these functionalities. The findings are presented in the subsequent sections.

Side-by-side analysis of the ^{13}C MAS NMR spectra (Fig. 3) revealed no discernible differences between the control and modified samples. Signals with characteristic chemical shifts 5were identified: signals δ 26.08, δ 28.83, δ 29.38 and δ 32.69 ppm from carbon atoms in the octamethylene chain, a δ 60.94 ppm signal from carbon atoms of the –CH_2 group attached to an unsubstituted hydroxyl group, a broad δ 65.01–66.82 ppm signal from the carbon atoms of the octamethylene –CH_2 alkyl groups closest to the ester bond and δ 43.43 and δ 73.28 ppm signals

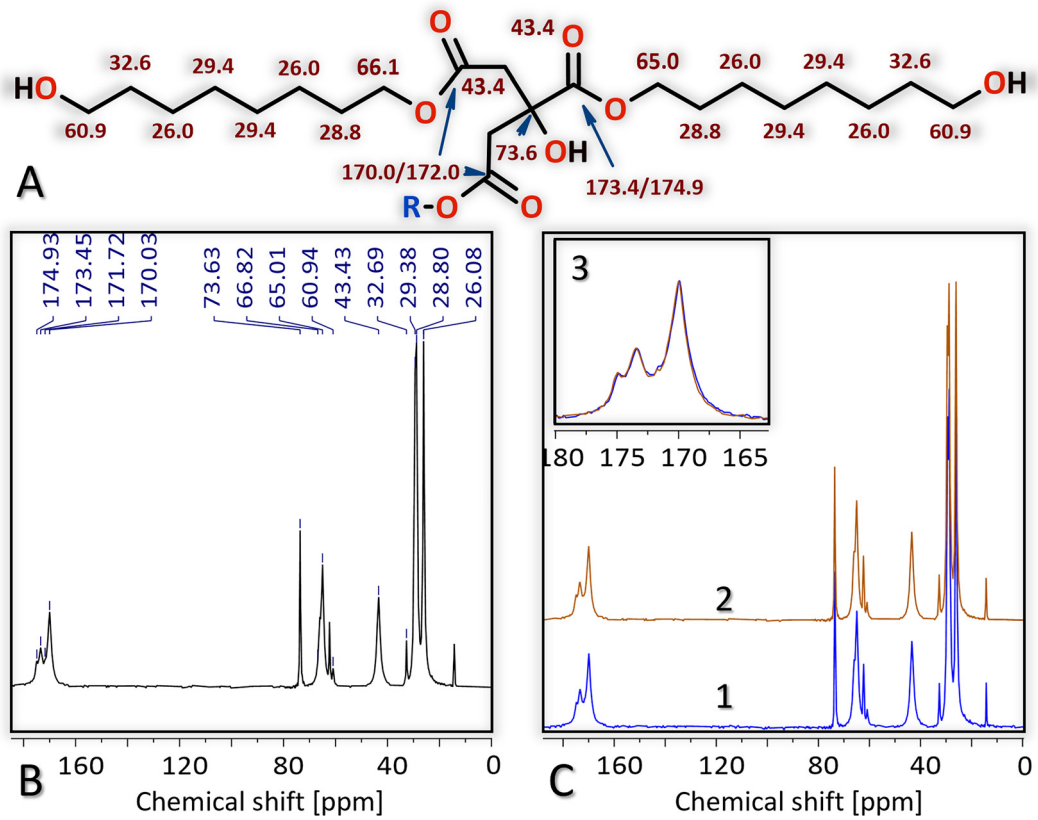

Fig. 3 Fragment of POC prepolymer structure along with chemical shift assignments based on ^{13}C MAS NMR analysis (A),^{13}C MAS NMR spectra obtained for the cPOC_2 : 3_4d_C with chemical shift assignments of the observed signals (B) and comparison of cPOC_2 : 3_4d_C and cPOC_2 : 3_4d_G0.8 spectra (C1) and (C2) and a close-up of the superimposed integrals of the carboxylic acid region of both spectra (C3).

from the citrate carbon atoms (from the $-CH_2$ groups and the central quaternary carbon, respectively) along with superimposed signals from substituted and unsubstituted carbonyl carbons in the range of δ 170.03–δ 174.93 ppm (Fig. 3A and B). In addition, a signal associated with triethyl citrate was identified (δ 14.86 ppm). Importantly, no new signals were detected for the cPAC_2:3_4d_G0.8 modified material (Fig. 3C1–C3) beyond those observed in the control samples, indicating that the incorporation of the modifier did not alter the material's overall chemical structure. The concentrations of both intact GSH molecules and the *in situ*-formed GSH-derived fluorescent compound were insufficient for detection by solid-state NMR spectroscopy. This observation is further supported by molar ratio and reactivity calculations (Fig. S1–S3, ESI†).

The close similarity between the spectra suggests that the addition of GSH at the tested concentrations does not affect the primary structure of the crosslinked cPAC materials. Despite the formation of a fluorescent compound within the network, the ratio of citrate to alkylene residues and the degree of –COOH group conversion remained unchanged (Fig. 3 and Fig. S2, ESI†). It can therefore be concluded that the quantity of unsubstituted carboxyl groups remained relatively constant throughout the reaction.

2.1.2.2. Fluorescence and antioxidative properties of the G_cPACs. The absence of significant alterations in the degree of conversion may also be explained by the mechanism of fluorophore formation. The fluorescence of the modified cPAC materials arises from the *in situ* formation of a fluorescent compound derived from GSH and CA, known as CTPC—3-[(carboxymethyl)carbamoyl]-5-oxo-2,3-dihydro-5*H*-[1,3]thiazolo[3,2-*a*]pyridine-7-carboxylic acid (Fig. 4A)—a non-toxic, biocompatible fluorophore with a maximum emission wavelength at 444 nm.[47] As demonstrated in our previous study,[47] this reaction occurs between CA molecules and the glycyl-cysteinyl dipeptide, which is formed *via* amide bond cleavage of the GSH molecule, accompanied by the release of the L-glutamic acid moiety (Fig. S4, ESI†). A similar reaction takes place during the crosslinking of G_cPAC materials, involving citrate groups and GSH hydrolysis products formed under the reaction conditions.

The formation of fluorophore molecules at the terminal ends of polymer chains imparts fluorescent properties to the materials while consuming a portion of free carboxyl groups. However, since each fluorophore introduces an additional terminal carboxyl group, the overall degree of conversion remains comparable between modified and unmodified samples.

UV-Vis and spectrofluorimetric analyses confirmed the fluorescent properties of the materials. In general, the samples exhibited blue fluorescence, with intensity increasing proportionally to the GSH concentration (Fig. 3B and C).

Characteristic photoluminescence (PL) emission bands with a pronounced maximum at 444 nm were observed, corresponding well with the emission spectra of pure CTPC, thereby supporting the *in situ* formation of this fluorophore under crosslinking conditions. Although the fluorescence intensity increased with higher GSH concentrations, the relationship was not linear. This nonlinearity suggests an uneven conversion of GSH to the fluorophore, potentially influenced by several factors.

First, the low dispersion of the modifier (less than 1% v/v in the material) significantly reduces the likelihood of condensation reactions between cysteinyl residues and available citrate groups. For the reaction to occur, a GSH molecule must encounter a sterically favorable citrate moiety with only one carboxyl group blocked. Additionally, the blocked group should not be one of the terminal carboxyl groups of the citrate residue, as closure of the six-membered anhydride ring—necessary for CTPC formation—would otherwise be implausible.[47] Furthermore, GSH must undergo thermally induced hydrolysis into a glycyl-cysteinyl dipeptide, which can then react with the citrate residue. The crosslinking temperature (80 °C) may only induce hydrolysis and subsequent reaction in a fraction of GSH molecules.

This interpretation is supported by the antioxidant properties observed for the tested materials, which result from the presence of unreacted GSH and its hydrolysis products within the polymer matrix. Additionally, fluorescence quenching mechanisms and internal filter effects likely interfere with the observed PL emission. A high polymer network thickness can scatter the excitation beam, decreasing the probability of molecular excitation and consequently lowering fluorescence intensity, especially in polyesters with lower fluorophore concentrations.

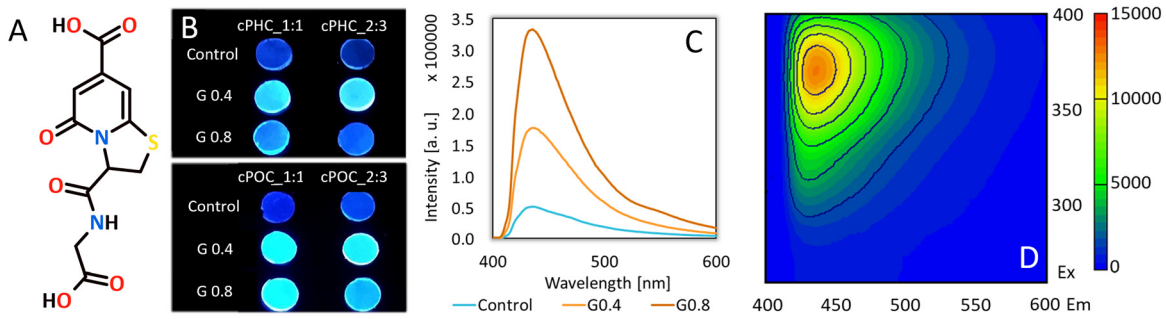

Fig. 4 The structure of CTPC fluorophore (A),[47] samples of control and modified cPAC materials under a UV lamp (B), photoluminescence (PL) emission spectra for control and modified cPHC_1:1_10d materials (C), and 3D fluorescence map for cPHC_1:1_10d_G0.8 (D).

Collectively, these factors contribute to the observed fluctuations in fluorescence intensity.

Importantly, these fluctuations do not obscure the clear influence of the diol type and reactant molar ratio on fluorescence intensity. The PL spectra show a distinct decrease in emission for materials prepared at a 2 : 3 CA : diol ratio compared to those at a 1 : 1 ratio. This decrease can be attributed to a higher molar excess of citrate residues in the 1 : 1 ratio materials, which enhances the probability of dipeptide–citrate reactions. Moreover, materials prepared at a 1 : 1 molar ratio were more acidic, which likely facilitated peptide bond cleavage in the GSH molecule, promoting fluorophore formation.

The type of diol used also influenced PL emission: materials synthesized with 1,6-hexanediol exhibited higher fluorescence than those synthesized with 1,8-octanediol. This effect can be explained by two factors: (1) the shorter alkylene chain in cPHC materials results in a higher molar density of citrate residues, and (2) the increased hydrophilicity of hexanediol-based materials compared to octamethylene-based ones, enhancing their reactivity with the hydrophilic glycyl-cysteinyl dipeptide.

The effect of crosslinking time on PL intensity was also investigated. Materials crosslinked for 10 days (10d) displayed the same trends described above, but with more pronounced differences. Prolonged crosslinking increased fluorescence intensity in materials with a higher probability of reaction occurrence (*e.g.*, cPHC_1 : 1). However, in materials with lower citrate content (2 : 3 molar ratio), prolonged crosslinking led to increased crosslinking density, greater blocking of carboxyl groups, and reduced hydrophilicity, ultimately resulting in decreased PL intensity.

The most substantial decrease in emission was observed for cPOC_2 : 3_10d, which, due to its longer octamethylene chain and consequently the lowest molar proportion of citrate groups, displayed the lowest hydrophilicity among all tested samples.[49]

As previously discussed, the introduction of the GSH tripeptide into the polyester structure occurs *via* two distinct pathways. The first involves the formation of a fluorescent derivative through the reaction of thermally hydrolyzed GSH fragments with citrate residues, as described above. The second pathway entails the incorporation of unreacted GSH into the polymer network. In this latter case, GSH molecules can be immobilized within the polymer matrix through either non-covalent interactions or covalent bonding (Fig. 5).

During the crosslinking process, GSH molecules can become physically encapsulated between network junctions or, owing to the presence of carboxyl and amino groups in the glycyl and glutamyl moieties, can undergo esterification and amidation reactions. As a result, GSH molecules can be covalently attached to alkylene or citrate groups at the ends of polymer chains (Fig. 5). In both cases, the antioxidant functionality of GSH is preserved, as the thiol groups in the cysteinyl residues—critical for the scavenging of reactive oxygen species (ROS)[50,51]—remain unreacted. Consequently, the material acquires new functionality, namely, the ability to neutralize free radicals.

The incorporation of antioxidant molecules into the polymer network can significantly mitigate oxidative stress, thereby reducing the risk of scaffold rejection and inflammation. To evaluate the antioxidant properties of G_cPAC materials, their ability to scavenge radicals was assessed using the 2,2-diphenyl-1-picrylhydrazyl (DPPH) assay. The results clearly demonstrated a decrease in absorbance values with increasing GSH content, confirming the antioxidant potential of the modified materials (Fig. 6).

The observed decrease in the absorbance of the tested solutions was influenced by both the molar ratio of the reactants and the curing time of the materials. Materials prepared at a 1 : 1 (CA : diol) molar ratio exhibited superior antioxidant properties compared to those obtained at a 2 : 3 ratio. This effect can be attributed to the higher hydrophilicity of the 1 : 1 (CA : diol) materials, resulting from a greater proportion of citrate residues relative to alkylene chains. Higher hydrophilicity facilitates greater DPPH penetration into the polymer network, thereby enhancing antioxidant activity.

Conversely, our previous research demonstrated that materials synthesized with a 2 : 3 (CA : diol) ratio provided a more favorable environment for adipose-derived stem cells (ASCs) and vascular smooth muscle cells (SMCs) growth, both in material extracts and during direct contact cultivation.[24] This was attributed to the lower acidity of 2 : 3 (CA : diol) materials compared to those synthesized at a 1 : 1 ratio.[24,48]

Discrepancies were also observed between materials crosslinked for 4 and 10 days. Longer crosslinking times led to higher absorbance values, indicating diminished antioxidant properties.

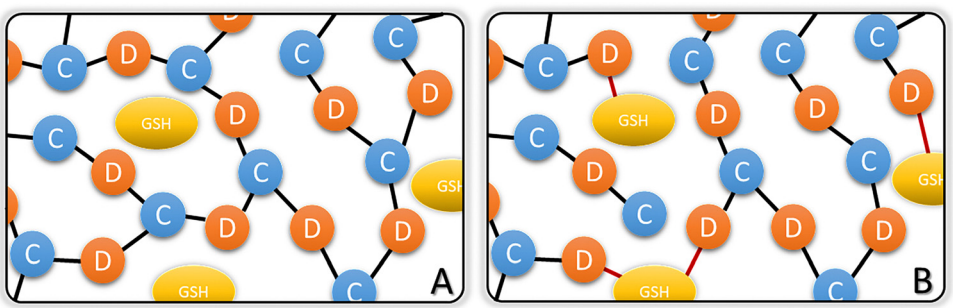

Fig. 5 Graphical representation of two possible ways of embedding the GSH molecules into cPAC materials: (A) non-covalent imparting between polymer chains, (B) covalent bonding to the available carboxyl and hydroxyl groups at the end of polymeric chains.

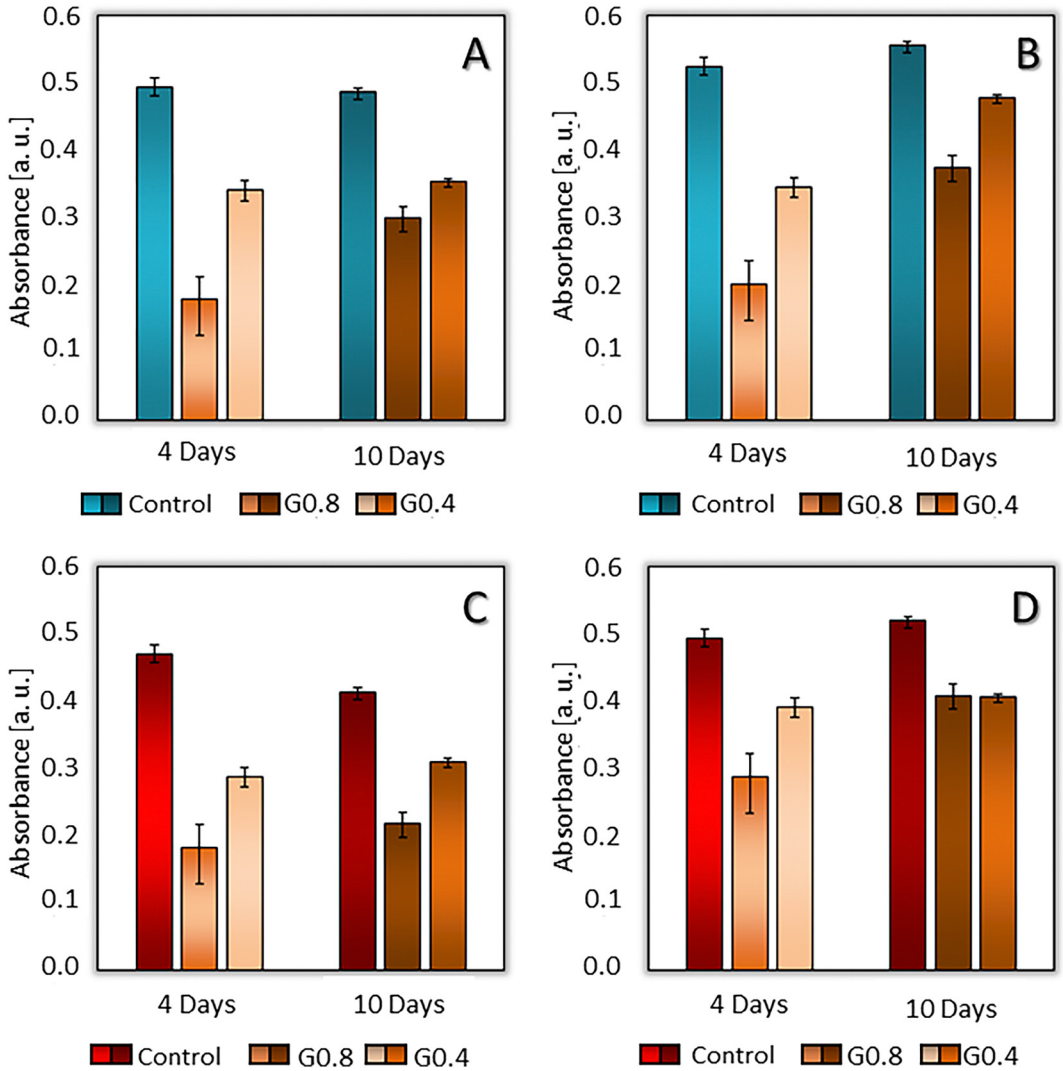

Fig. 6 Comparison of the antioxidant properties of modified PAC materials depending on the length of crosslinking time. (A) cPHC_1 : 1, (B) cPHC_2 : 3, (C) cPOC_1 : 1, (D) cPOC_2 : 3. Absorbance was measured at 517 nm.

This phenomenon can be explained by the increased crosslinking density, which hinders DPPH diffusion into the polymer network and thus reduces its radical scavenging efficiency. Interestingly, the type of diol used had no significant effect on absorbance, suggesting that crosslinking density is the primary factor influencing the antioxidant performance of the materials.

These findings confirm the successful introduction of two new functionalities into PAC materials: fluorescence and antioxidant properties. GSH incorporation into the polymer network proceeds *via* two mechanisms: (1) reaction between citrate and cysteinyl moieties, leading to the formation of a fluorescent product (CTPC); and (2) physical encapsulation and covalent attachment of intact GSH molecules, which are responsible for ROS-scavenging activity.

Specifically, the antioxidant activity arises from the well-known reaction of GSH with ROS, resulting in the formation of glutathione disulfide (GSSG),[52] a dimer linked by disulfide bonds between cysteinyl thiol groups. In contrast, GSH residues that participate in CTPC formation have their thiol groups blocked, rendering the fluorophore incapable of antioxidant action.

These observations suggest that unreacted GSH and its hydrolysis products capable of disulfide bond formation are effectively retained within the G_cPAC network. As the scaffold degrades over time *in vivo*, a gradual release of GSH is expected, providing a sustained antioxidant effect beneficial for surrounding cell proliferation—a highly promising feature for soft tissue engineering applications.

Notably, the relatively low GSH content used in material synthesis proved sufficient to significantly reduce DPPH radicals, while having no substantial effect on the mechanical properties of the materials, as confirmed by additional analyses (Fig. S5–S7, ESI†).

2.1.2.3. Dynamic-mechanical and thermal analysis of the G_cPACs. The influence of GSH addition on thermo-mechanical behavior of the crosslinked samples was studied using dynamic-

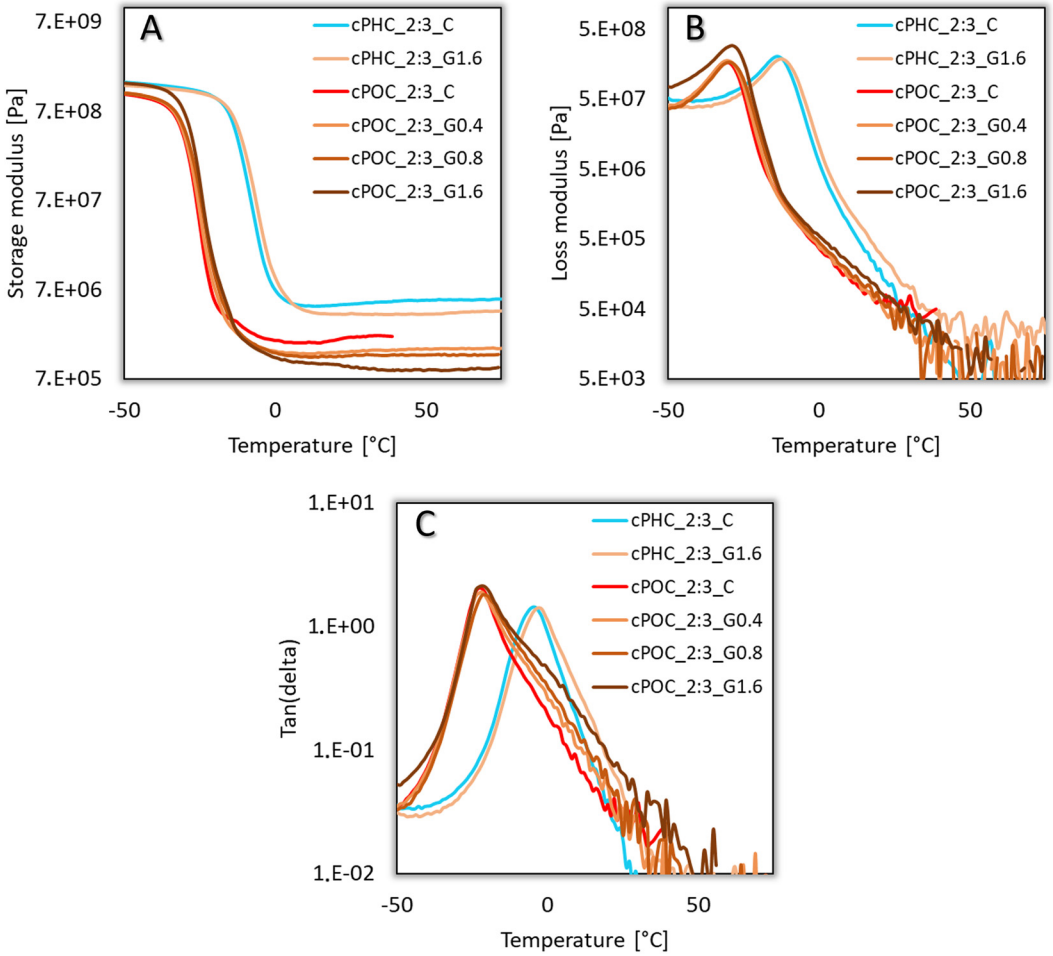

Fig. 7 DMTA results showing evolution of storage moduli (A), loss moduli (B), and loss factor (tan δ) (C).

mechanical and thermal analysis (DMTA). The DMTA curves confirmed the formation of chemical networks in all samples, which is evidenced by the appearance of a rubber plateau (above T_α) on the G' curves (Fig. 7).

The PHC samples show both higher T_α and the storage modulus at rubber plateau (G'_R values) than POC, which results from their higher cross-link density (ν_e, Table 1). In the case of PHC series, shorter hexamethylene chains are built into the network structure, therefore their calculated ν_e values are higher than those of the POC series with longer octamethylene chains. Surprisingly, the GSH addition had no significant effect on T_α (Table 1) for both PHC and POC series. This suggests that the GSH molecules interact strongly with the network chains and do not plasticize the final material. As previously shown in Fig. 5, these interactions can involve both non-covalent and covalent bonding of GSH molecules with the polymer network. The origin of these interactions was also partly revealed from DMTA. It can be seen that the G'_R values decrease with increasing GSH concentration, *i.e.* the cross-link density (ν_e) also decreases gradually, while T_α remains constant. This proves that when $T > T_\alpha$ is reached, the non-covalent bonds are disrupted, which is manifested by a decrease in the effective cross-link density, *i.e.* a decrease in G'_R, of the GSH-containing networks.

Table 1 DMTA results showing main transition temperature (T_α), storage modulus at rubber plateau (G'_R) and calculated effective cross-link density (ν_e)

Sample ID	T_α, °C	G'_R, MPa	ν_e, mmol cm^{-3}
cPHC_2:3_C	−5	5.4	2.04
cPHC_2:3_G1.6	−3	3.7	1.39
cPOC_2:3_C	−23	2.1	0.84
cPHC_2:3_G0.4	−22	1.4	0.56
cPOC_2:3_G0.8	−21	1.3	0.52
cPOC_2:3_G1.6	−22	0.9	0.36

2.1.2.4. In vitro tests of antioxidant activity of modified cPACs. The first experiment (Fig. 8) was designed to compare the proliferation and viability of human adipose tissue-derived stem cells (ASCs) in culture on cPOC_2:3_10d and cPHC_2:3_10d materials modified with four different concentrations of GSH, *i.e.*: 0, 0.4, 0.8, and 1.6% v/v. The reason for selecting ASCs was their relatively easy availability through liposuction of the patient's subcutaneous tissue and their suitability to

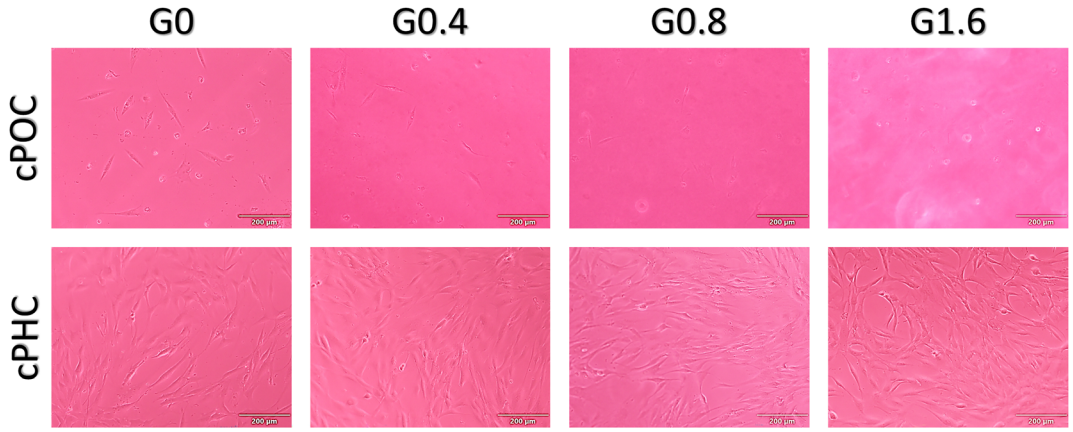

Fig. 8 Comparison of the survival and proliferation of human ASCs in 3-day-old cultures on cPOC_2 : 3_10d or cPHC_2 : 3_10d endowed with GSH (G) at concentrations of 0.0, 0.4, 0.8 and 1.6% w/w. Native cultures, Olympus IX71 microscope, obj. 10×, bright field, scale bar 200 μm.

reconstruct blood vessels, specifically by differentiating into smooth muscle cells (SMCs).[53] The selection of polymers with a molar ratio CA : diol of 2 : 3 was made due to its lower acidity than that of 1 : 1, as demonstrated in our prior research[24] and confirmed in the present study.

The results showed that, in contrast to cPHC_2 : 3_10d, cPOC_2 : 3_10d materials showed poor performance in terms of cell proliferation and biocompatibility. After 3 days of cell cultivation, cPOC_2 : 3-based substrates contained low numbers of sparse cells, while ASCs were subconfluent on cPHC_2 : 3-based materials (Fig. 8). Even prolonged rinsing of the cPOC-based materials with the culture medium prior to cell seeding did not prevent the release of potentially cytotoxic substances into the medium. High acidity was detected in this medium, which contained phenol red as pH indicator, suggesting the release of unreacted CA from cPOC. Similar cell behavior was observed in the previous study[24] with ASCs cultured in extracts of cPOC_2 : 3_10d and cPHC_2 : 3_10d in the cell culture medium. While undiluted extracts of cPHC_2 : 3_10d allowed ASCs adhesion, spreading and subsequent growth (up to day 7 of cultivation), the cells did not adhere and proliferate in undiluted extracts of cPOC_2 : 3_10d. Thus, for subsequent experiments with different GSH concentrations, the cPHC_2 : 3_10d was selected.

The biocompatibility of cPHC_2 : 3_10d materials with increasing GSH concentration was tested on four cell types, namely the aforementioned human ASCs, normal neonatal human dermal fibroblasts (NHDFs), human umbilical vein endothelial cells (HUVECs), and human umbilical artery smooth muscle cells (SMCs). NHDFs, HUVECs and SMCs represent the major cell types in the vascular wall, *i.e.* fibroblasts in the tunica adventitia, endothelial cells in the tunica intima and smooth muscle cells in the tunica media, thus making these cell types relevant for vascular tissue engineering. Although all cell types monitored grew generally better on tissue culture polystyrene (TCPS) than on cPHC_2 : 3_10d materials, *i.e.* were more homogeneously distributed with higher cell population densities (Fig. 9), strong adhesion and subsequent

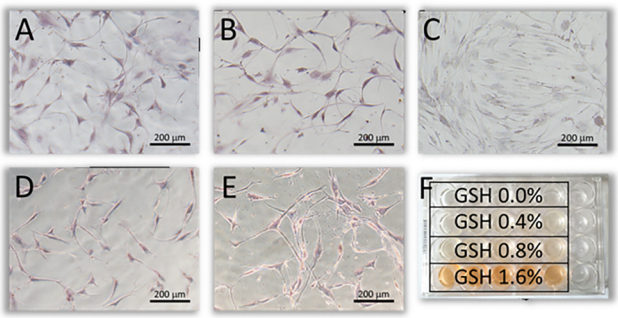

Fig. 9 Comparison of the cell population density and morphology of human ASCs in 3-day-old cultures on cPHC_2 : 3_10d modified with GSH in concentrations of 0.0 (A), 0.4 (B), 0.8 (D), and 1.6 (E) % w/w, and on control TCPS (C). Cells were fixed with 4% paraformaldehyde and stained with hematoxylin and eosin. Olympus IX71 microscope, obj. 10×, bright field, scale bar 200 μm. (F) Distribution of GSH-modified cPHC_2 : 3_10d in a 24-well tissue culture plate. The increasing concentration of GSH is evident by the gradual color change of the material from colorless to orange. The last column on the right in the plate represents the control TCPS.

proliferation was also observed on cPHC_2 : 3_10d for each monitored cell type and all GSH concentrations tested (Fig. 10).

As mentioned above, the idea of modifying cPHC with GSH arose from the well-described negative effects of oxidative stress on cell growth and viability. Therefore, menadione was chosen as a substance that induces cell death through ROS-dependent mechanisms.[54] Initially, preliminary tests were performed with menadione concentrations ranging from 50 μM to 500 mM on ASCs seeded on control and GSH-modified cPHC materials. Although not all data are presented in this paper, a representative example of the effect of menadione at the highest concentration of 500 mM on cell viability and metabolic activity is shown in Fig. 11.

As determined by the resazurin assay, cell metabolic activity was higher on TCPS than on cPHC_2 : 3_10d samples without and with GSH prior to menadione treatment. After 1 hour of preincubation of the cell on the tested samples with 500 mM

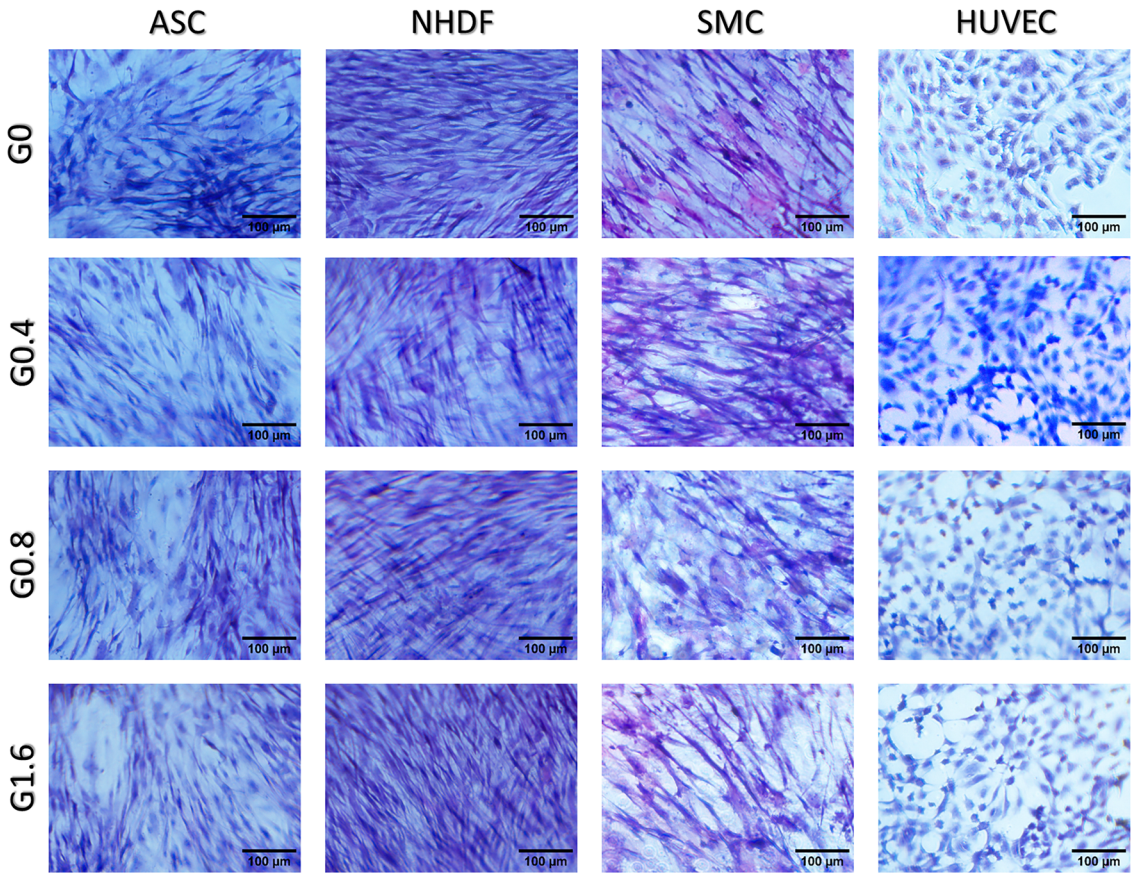

Fig. 10 Comparison of the cell population density and morphology of four cell types, namely ASCs, NHDFs, SMCs and HUVECs on day 4 after seeding on control cPHC_2 : 3_10d material without GSH (G0), and on cPHC_2 : 3_10d with increasing GSH (G) concentration of 0.4, 0.8 and 1.6% w/w. Cells were stained with hematoxylin and eosin. Olympus IX70 microscope, objective 10×, bright field, scale bar 100 µm. It is evident that the tested materials provided suitable substrates for the growth of ASCs and NHDFs in particular. In the case of HUVECs and SMCs, the increasing concentration of GSH is rather limiting for cell growth.

menadione, the cell metabolic activity as measured by a resazurin assay decreased in all samples. However, this decrease was least evident in cPHC_2 : 3_10d with the highest GSH concentration, *i.e.* 1.6% v/v. At 2 h after preincubation with menadione, cell metabolic activity continued to decrease in all samples, reaching similarly low levels on TCPS and on cPHC_2 : 3_10d with 0.0–0.8% GSH. The exception was sample cPHC_2 : 3_10d with 1.6% GSH, where the cell metabolic activity was the highest of all monitored samples. Thus, a certain protective effect of GSH against oxidative stress became apparent only at the highest GSH concentration tested (Fig. 11).

The decrease in metabolic activity of ASCs following the addition of 500 mM menadione was accompanied by morphological changes in these cells. Fig. 12 shows the response of ASCs grown on cPHC_2 : 3_10d without GSH and with increasing concentrations of GSH (0.4%; 0.8%; 1.6% w/w) and control TCPS to the addition of 500 mM menadione. Prior to the addition of menadione (Fig. 12), cells were elongated and well adherent to all substrates tested. After the addition of menadione (Fig. 12), the cells began to round and detach from the culture substrate, a sign of their reduced viability, which is particularly evident on cPHC_2 : 3_10d without GSH (Fig. 12). However, this cell behavior is less pronounced on cPHC_2 : 3_10d with GSH, indicating a protective effect of GSH on the cells (Fig. 12).

In the final step, a relatively low concentration of menadione of 500 µM was selected for the following tests, since this concentration has been shown to cause moderate oxidative effects on cells, comparable to common physiological conditions. Therefore, the viability of four cell types, *i.e.* ASCs, NHDFs, HUVECs and SMCs, cultured on cPHC_2 : 3_10d with increasing concentrations of GSH and exposed to 500 µM menadione was compared. Cell viability was measured using the metabolic resazurin assay. A control measurement without menadione was performed at the beginning of the experiment. This was followed by the application of 500 µM menadione for three hours, and after three hours, another resazurin assay was performed in the presence of menadione. The principle of the resazurin assay is based on the reduction of blue (oxidized) resazurin to the pink (reduced) product resorufin by oxidoreductase enzymes in the mitochondria and cytosol of metabolically active cells. Therefore, the assay may interfere with the antioxidant potential of the GSH present in the materials, and it was necessary to provide a relatively complex set of control

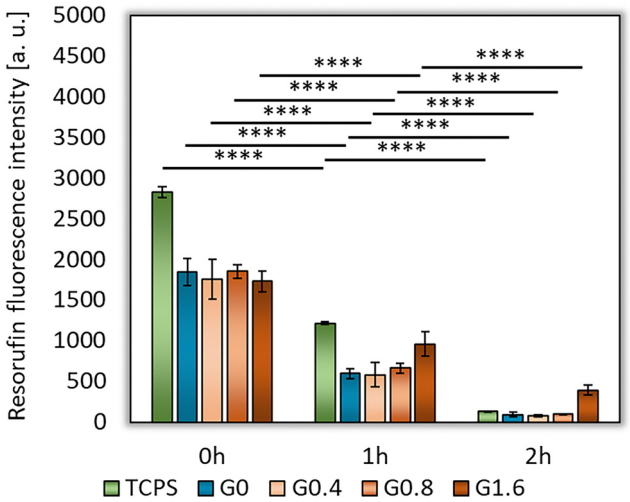

Fig. 11 Time-dependent effect of 500 mM menadione on cell survival and metabolic activity assessed by a resazurin assay in ASCs cultured on TCPS and cPHC_2 : 3_10d materials with increasing GSH (G) concentration from 0 to 0.4, 0.8 and 1.6% w/w. The cells were pre-incubated in menadione for 1 or 2 hours, and then they were incubated with a medium with resazurin and menadione for another 3 hours, *i.e.*, for 4 and 5 hours in total. Metabolic activity decreased significantly with the time of incubation. Only the cells on cPHC materials with the highest GSH concentration (1.6% w/w64) showed a more pronounced metabolic activity after 2 hours (*i.e.* 5 hours) of menadione treatment, but the difference between the 1(4)-hour- and 2(5)-hour responses to menadione is still significant. Data are presented as mean ± SD of 6 measurements, and two-way ANOVA analysis was performed. The Shapiro-Wilk test was performed for each data set. Values connected by lines differ significantly from each other (****$p < 0.0001$).

samples (see Materials and methods section, Chapter 4.4.2). The results of the resazurin assay are shown in Fig. 13.

Apparently, the metabolic activity of cells after menadione application is strongly influenced by the composition of the cultivation substrate and the cell type. The most pronounced antioxidant effect of GSH, together with high cell sensitivity to oxidative stress, was observed in ASCs (Fig. 13A). These cells exhibited a significant decrease in metabolic activity on all media tested after exposure to 500 μM menadione, although this reduction was less pronounced on media with higher GSH concentrations, indicating an antioxidative effect of GSH-enriched samples. Similar results were also obtained when the cell viability was assessed using the CellTiter-Glo® luminescent cell viability assay. This assay allows for the measurement of the product of cellular metabolism not only in the culture medium, as in the case of the resazurin assay, but also in the lysates of cells previously grown on the tested materials. We found that the viability of ASCs was significantly higher in cells cultured on all samples tested without exposure to menadione than in the presence of menadione (Fig. 14).

On the one hand, when cell viability was compared on cPHC materials with different GSH concentrations, this value was significantly higher on the material with 1.6% w/w GSH than on the material with 0, 0.4 and 0.8% w/w GSH, indicating a positive influence of the material functionalization with GSH on cell viability. On the other hand, on all cPHC_2 : 3_10d materials, even those without GSH, the cell viability was significantly higher than in control plastic wells, especially in cells exposed to menadione. This result indicates a positive effect of the cPHC-based material itself on cell viability, more or less independent of the presence of GSH. One explanation is that the cPHC-based material probably had an inherent antioxidant effect, similar to that of the other related citric acid-based materials. Examples of these materials are as poly(1,8-octamethylene citrate) (POC), which has been used to mitigate the oxidative properties of superparamagnetic iron oxide nanoparticles (SPIONs) used for non-invasive visualization of engineered endothelium in vascular grafts,[55] poly(octanediol-citrate-polyglycol), which improved skin wound healing and polarized macrophages to an anti-inflammatory M2-phenotype[56] or a biodegradable thermoresponsive gel copolymer of citric acid, poly(ethylene glycol) (PEG), and poly-*N*-isopropylacrylamide (PNIPAAm).[57]

In addition to ASCs, a relatively high sensitivity to oxidative stress was also observed in NHDFs (Fig. 13B), but in this case,

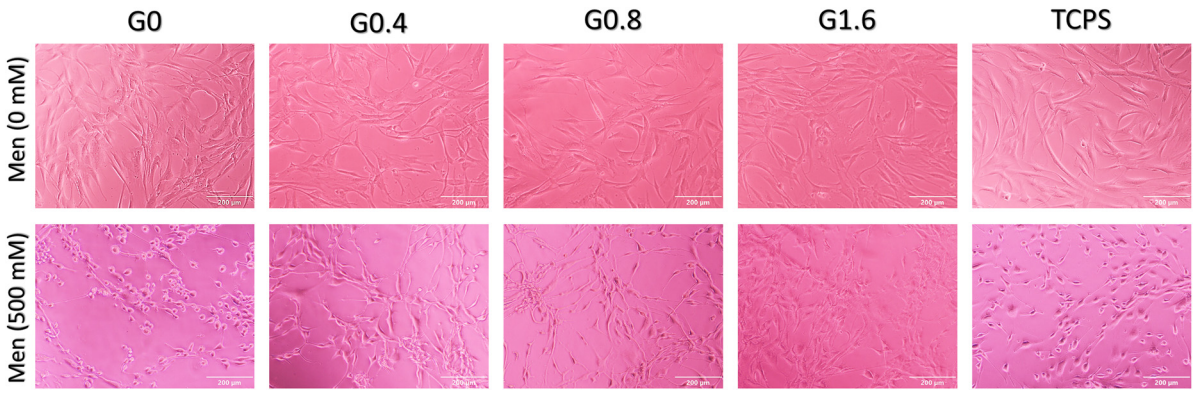

Fig. 12 Comparison of the cell population density and morphology of ASCs seeded on cPHC_2 : 3_10d material with increasing GSH (G) concentrations from 0 to 0.4, 0.8 and 1.6% w/w and control TCPS. Cells were either untreated or pre-treated with 500 mM menadione (Men) for 2 hours. Native cultures, Olympus IX70 microscope, objective 10×, bright field, scale bar 200 μm. Obviously, ASCs seeded on materials without GSH did not adhere well under the oxidative stress. However, a positive influence of the antioxidant effect of GSH on cell morphology can be seen.

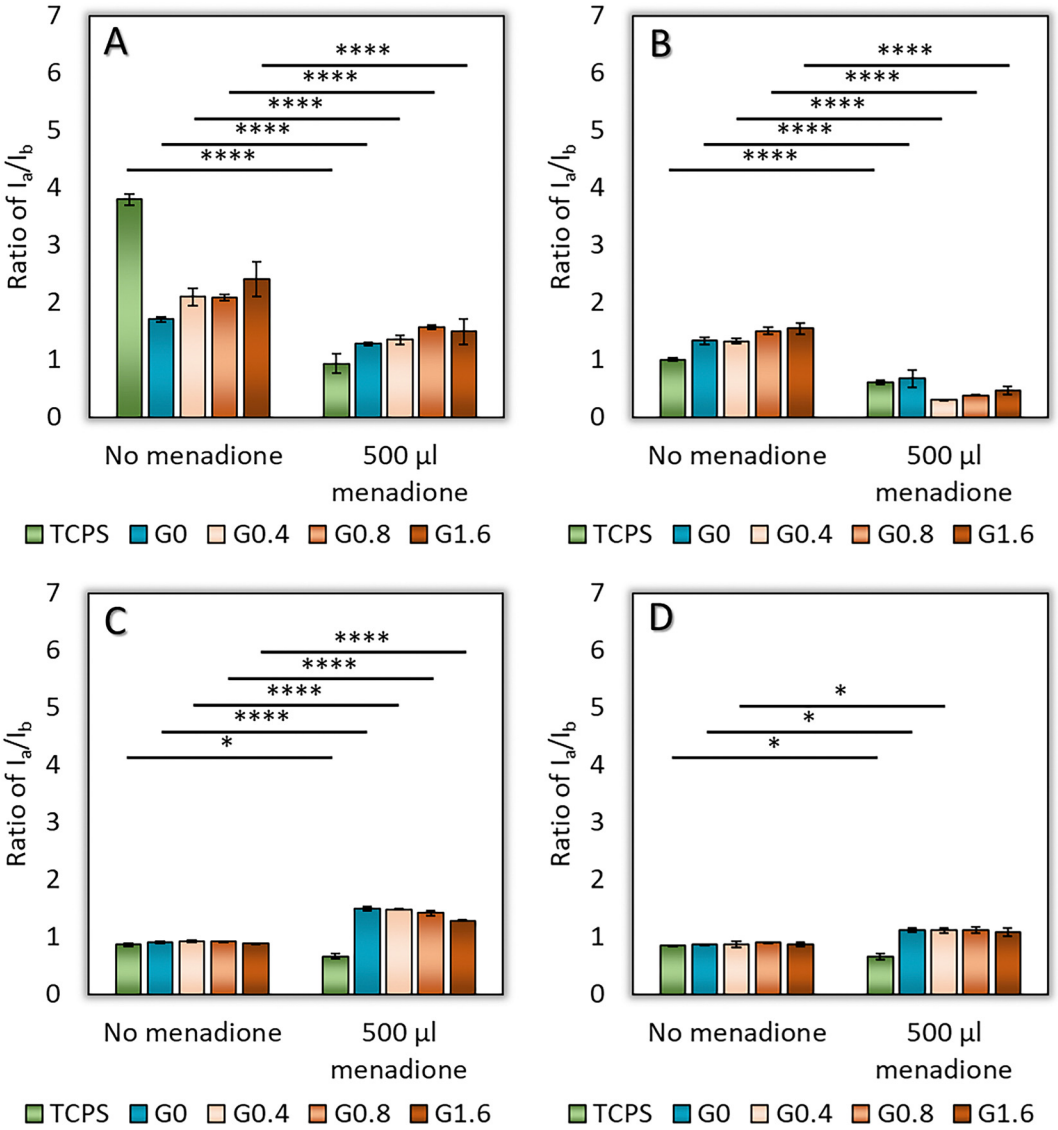

Fig. 13 The influence of GSH content in the cPHC_2 : 3_10 material on cell survival and metabolic activity (resazurin assay) under the oxidative stress (after 6 hours of menadione treatment). (A) ASCs, (B) NHDFs, (C) HUVECs, (D) SMCs. Cells were cultured on TCPS, on the materials without GSH (G0) and with GSH (G) content of 0.4, 0.8 and 1.6% w/w. Data are presented as the ratio of the fluorescence intensity of resorufin after incubation of cells with menadione (I_a) to the fluorescence intensity of resorufin before incubation of cells with menadione (I_b). The ratio (R) is expressed as the mean ± SD of 3 and 6 measurements for samples without and with menadione, respectively. $R = 1$ indicates that the metabolic activity of the cells after incubation with menadione is the same as before incubation; $R > 1$ indicates that this metabolic activity is higher, and $R < 1$ indicates a decrease in the cell metabolic activity after incubation with menadione. Two-way ANOVA analysis with the Shapiro-Wilk test was performed for each data set. Values connected by lines differ significantly from each other (****$p < 0.0001$; ***$p < 0.001$; **$p < 0.01$; *$p < 0.05$).

the antioxidative effect of GSH-enriched samples was less evident. Even in GSH-enriched samples, cell metabolic activity after incubation with menadione was lower than before incubation and lower than in menadione-free samples, which again suggests the intrinsic antioxidative capacity of cPHC materials. However, the response of HUVECs and SMCs (Fig. 13C and D) to menadione application was opposite to that of ASCs and NHDFs – the metabolic activity of these cells, especially HUVECs, actually increased significantly after menadione application. A potential explanation may be that cells of the vessel wall, particularly endothelial cells that form the inner lining of the vessel, are in the first line to encounter oxygen radicals from the blood (*e.g.*, from activated immune cells). Therefore, these cells may be more resistant to oxidative damage than cells that are physiologically more distant from the vessel lumen, such as fibroblasts or ASCs. Endothelial cells and their progenitors show relatively high expression and activity of antioxidant enzymes, such as nicotinamide *N*-methyltransferase,[58] AD(P)H dehydrogenase [quinone] 1,[59] or manganese superoxide dismutase.[60] Under oxidative stress, endothelial cells can also undergo endothelial-mesenchymal transition, *i.e.* they acquire an SMC-like phenotype, and

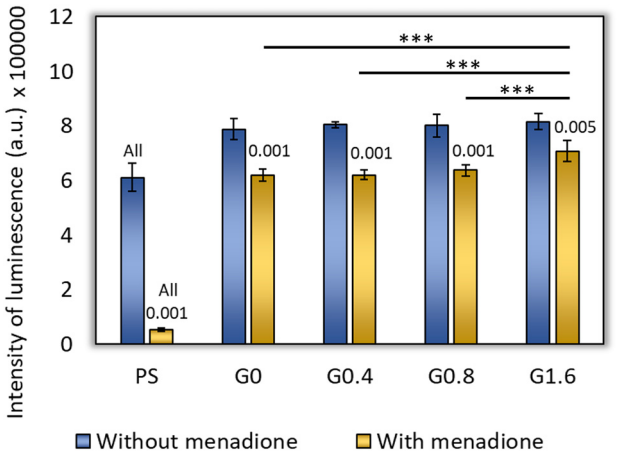

Fig. 14 The viability of ASCs, measured by the CellTiter-Glo® luminescent cell viability assay, in Nunclon™ Delta surface polystyrene (PS) plates and on cPHC_2 : 3_10d materials with GSH (G) content of 0, 0.4, 0.8, or 1.6% w/w, without menadione, or after 2 hours exposure to 100 μM menadione added to the culture medium. Data are expressed as mean ± SD (n = 4). Statistical significance: 0.001, 0.005: significantly lower ($p \leq 0.001$ or $p \leq 0.005$) compared to cells on the same material not exposed to menadione (Student t-test). All: significantly lower ($p \leq 0.001$; ANOVA, Student–Newman–Keuls method) compared to cells on all corresponding materials (*i.e.*, either non-exposed or exposed to menadione). ***: significantly higher ($p \leq 0.001$; ANOVA, Student–Newman–Keuls method) compared to cPHC with 0, 0.4, and 0.8% w/w GSH.

proliferate.[61] Oxygen radicals not only damage the cells and cause cell senescence and death, but at moderate concentrations, they can also directly stimulate the proliferation of cells, including endothelial cells and SMCs, by a mechanism similar to that of growth factors (for a review, see ref. 54 and 62). As early as 1996, Burdon hypothesized that normal production of ROS is necessary for normal transduction of signals that regulate cell growth.[63]

Interestingly, in HUVECs, increasing GSH concentrations even resulted in a slight reduction in the cell metabolic activity, although this reduction was not significant (Fig. 13C). It is known that the metabolic activity of cells is often directly proportional to the number of cells, *i.e.* it is even considered an indicator of cell proliferative activity.[64] Thus, this result could confirm our hypothesis that in the case of HUVECs, oxygen radicals indeed stimulated the proliferation of these cells. Another reason could be some adverse effect of high GSH concentrations on the cells, especially in the presence of oxidizing agents. It is known that ROS can oxidize cellular GSH, which can lead to the loss of intracellular redox homeostasis and activation of the apoptotic signaling cascade.[65] Nevertheless, the cell-specific differences in the response to GSH-loaded cPHCs and oxidative stress need to be further investigated in more detail.

In the present study, the focus was maintained on ASCs, which have been demonstrated to be the most sensitive to oxidative stress induced by menadione and to GSH concentrations in the cPHC material. Furthermore, ASCs are a promising stem cell type for vascular tissue engineering. The generation of ROS in ASCs using the ROS Detection Assay Kit (DFCDA/H_2DCFDA) was monitored. The principle of the test is that after diffusion of H_2DCFDA into the cells, the acetyl groups on this compound are cleaved by intracellular esterase to yield a non-fluorescent compound, which is oxidized by ROS to highly fluorescent 2′,7′-dichlorodihydrofluorescein. Fluorescence is then detected from the bottom of 96-well glass-bottom plates. Therefore, this assay was performed in material extracts because the cells must adhere directly to the glass bottom of the wells and not to the material, whose fluorescence could additionally interfere with that of 2′,7′-dichlorodihydrofluorescein.

It was determined that the production of ROS occurred not only in cells that had been exposed to menadione, but also in unexposed cells. This finding may be indicative of the physiological ROS production necessary for signal transduction.[54,63] However, the ROS production was significantly higher in exposed than in unexposed cells (Fig. 15A). Although cells cultured in extracts of cPHC with 0.4 and 1.6% w/w GSH tended to produce less ROS than cells in control medium, these differences did not reach statistical significance. However, when ROS production in cells exposed to menadione was normalized to the ROS production of corresponding cells cultured without menadione, the resulting values in cells cultured in all extracts of cPHC material, including those without GSH, were significantly lower than in cells cultured in control medium (Fig. 15B). This again suggests an intrinsic antioxidant capacity of cPHC, similar to that in other citric acid-containing materials. For example, extracts of polyvinyl alcohol modified with citric acid showed protective effects on bone marrow mesenchymal stem cells under oxidative stress *in vitro*. These extracts enhanced the antiapoptotic capacity of stem cells by upregulating the nuclear receptor peroxisome proliferator-activated receptor γ (PPARγ) and manganese superoxide dismutase 2 (Mn-SOD2), which scavenges mitochondrial ROS.[66] Citric acid, together with protocatechuic acid, has been used as a protective antioxidant coating for magnetic nanoparticles incorporated into ASCs for their maneuverability and traceability in cell therapies, *e.g.*, for the potential treatment of hearing disorders in regenerative audiology.[67]

A potential intrinsic antioxidant capacity of the cPHC materials was further confirmed by other experiments performed in the material extracts, namely monitoring of the growth of ASCs exposed to menadione using the xCELLigence real-time cell analyzer. This system monitors cell growth by measuring the electrical impedance generated by cells adhering to the bottom of special culture plates with gold microelectrodes, which is presented as the cell index. The method of studying cell growth in extracts of the materials has already been used and proven successful in our previous study of cPOC and cPHC.[24] When the cells were exposed to menadione (15 μM), the cell index increased to higher values in extracts of materials than in control standard DMEM with supplements, and this increase was similar in extracts of materials without and with GSH at all concentrations tested (Fig. S8 in the ESI†), *i.e.* it was GSH-independent.

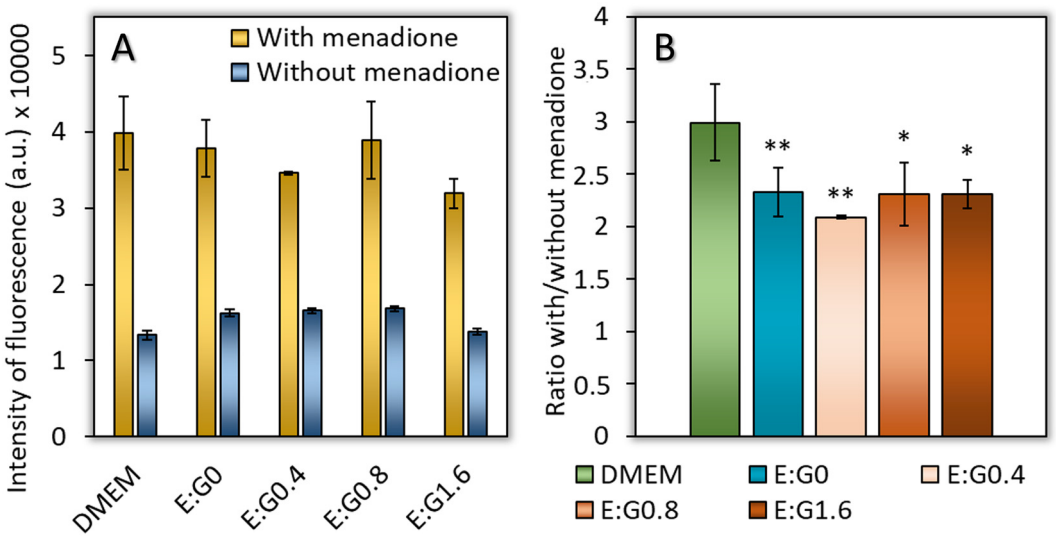

Fig. 15 Production of ROS in ASCs cultured in standard cell culture medium (DMEM) and in extracts (E) of cPHC_2 : 3_10d materials with GSH (G) content of 0, 0.4, 0.8, or 1.6% w/w, measured with the ROS Detection Assay Kit (DFCDA/H_2DCFDA). (A) Intensity of fluorescence of the cells with menadione added to the culture medium and without menadione. (B) The ratio between the intensity of fluorescence of cells cultured with menadione and the value in cells cultured without menadione. Mean ± SD (n = 3). ANOVA, Student–Newman–Keuls Method. Statistical significance: ** $p \leq 0.01$, *$p \leq 0.005$ compared to DMEM.

Moreover, cell indices in extracts with 15 μM menadione eventually reached slightly higher values than those without menadione. This is consistent with findings that oxidants at low levels can act as redox-active messengers in signal transduction pathways involved in responses to growth stimuli.[54] However, at higher levels, oxidants can cause damage to proteins, lipids, and nucleic acids, which can lead to cell death by apoptosis and/or necrosis.[54]

Taken together, both the ROS detection assay and xCELLigence growth monitoring demonstrated that the antioxidant and pro-cell growth effects of cPHC-based materials are rather independent of the presence and concentration of GSH in these materials. Interestingly, these results were most evident when cells were grown in extracts of the materials. When cells were grown directly on the materials, as in the resazurin or CellTiter-Glo® luminescent cell viability assay, some positive and concentration-dependent effect of GSH was seen. This suggests that when the materials were leached into the culture medium, it was primarily the citric acid-based components of the materials that were extracted into the medium rather than the GSH molecules. Another possibility is that GSH has lost its activity. GSH mitigates the effects of oxidants quickly and directly by oxidizing their sulfhydryl group, whereas citric acid may act long-term and indirectly by stimulating the synthesis of antioxidant enzymes and other molecules, including GSH.[68] Nevertheless, this issue needs to be further clarified, along with the positive influence of oxidative stress induced by a low concentration of menadione on ASC growth in the xCELLigence experiment (Fig. S8 in the ESI†) and on metabolic activity of HUVECs and SMCs seen in the resazurin assay (Fig. 12C and D).

2.1.2.5. In vitro tests of hemocompatibility of modified cPACs. The hemocompatibility of cPHC-based materials was evaluated by several methods, including direct contact with fresh human blood, with isolated erythrocytes to evaluate hemolysis, and the plasma recalcification test (PRT).

After direct contact with freshly collected heparinized human blood, the samples were analyzed by scanning electron microscopy (SEM) to study how blood cells adhere to the surfaces and form clots. This method allows us to observe the early thrombogenic processes that occur after biomaterial implantation. Fig. 16 shows representative SEM images of glass and tested materials after exposure to heparinized blood. A blood clot composed of platelets, leukocytes and fibrin is present on the glass surface. On the cPHC-based materials, only a few sparsely distributed non-activated leukocytes were detected. The images correlate with PRT data (see below) and indicate low thrombogenicity of the material.

The freshly drawn heparinized whole blood assays also included the assessment of markers of inflammation and complement activation by measuring polymorphonuclear (PMN)-elastase and soluble complement 5b-9 (sC5b-9) levels, respectively.[69] Elevated PMN-elastase levels indicate neutrophil activation, while elevated SC5b-9 levels serve as a sensitive marker of terminal complement pathway activation. Together, these parameters provide essential insight into the immune response induced by the biomaterial, ensuring its safety and suitability for clinical applications. Samples with 0.8 and 1.6% w/w GSH showed significantly elevated PMN-elastase levels (up to approx. 80 ng mL^{-1}) compared to the reference glass surface (approx. 40 ng mL^{-1}; Fig. 17A). However, this increase can still be considered low and rather negligible. In a study focusing on male infertility, the concentration of PMN-elastase in the serum of asymptomatic patients (n = 221) reached a median value of 127.7 ng mL^{-1}.[70] In addition, SC5b-9 levels were comparable for all materials tested and did not show significant complement activation (Fig. 17B).

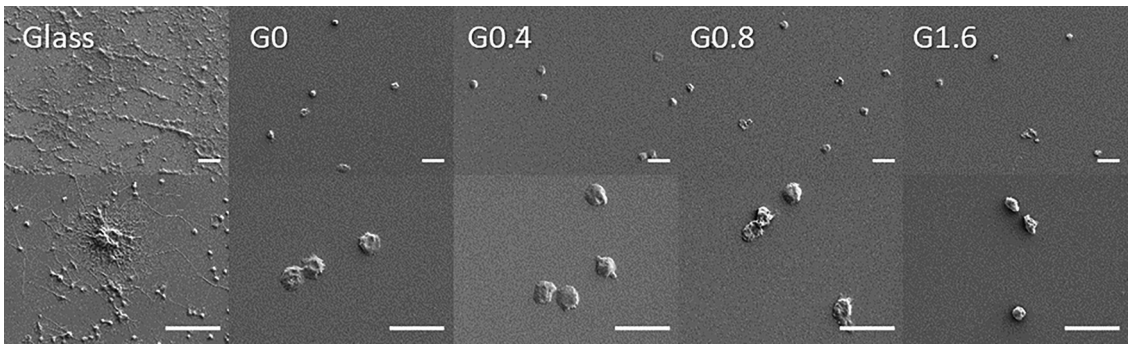

Fig. 16 Scanning electron microscopy (SEM) images of control microscopic glass coverslips (glass) and cPHC_2 : 3_10d materials with GSH (G) content of 0, 0.4, 0.8, or 1.6% w/w after 1 h incubation with fresh heparinized human blood at 37 °C. The scale bar is 20 μm.

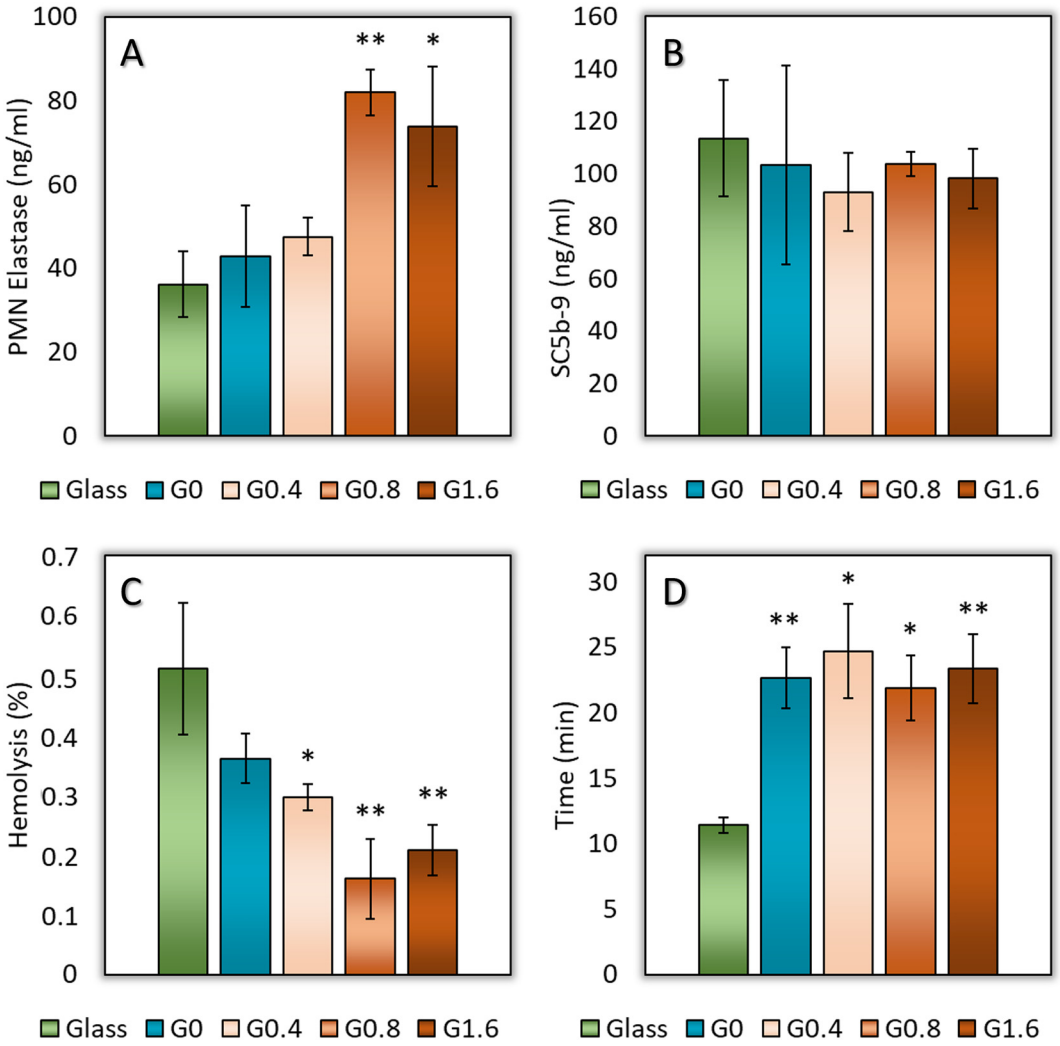

Fig. 17 Hemocompatibility of control microscopic glass coverslips (glass) and cPHC_2 : 3_10d materials with GSH (G) content of 0, 0.4, 0.8, or 1.6% w/w. (A) and (B) The tested samples were incubated with fresh human blood for 60 minutes at 37 °C. The levels of PMN-elastase, a marker of leukocyte activation (A) and SC5b-9, a marker of terminal complement complex formation (B), were then quantified by ELISA. (C) Hemolytic activity of the tested materials after contact with a 2% erythrocyte solution for 4 hours. (D) Plasma recalcification time after contact of the tested materials with human blood plasma recalcified with $CaCl_2$ (final concentration 0.02 M). Data are expressed as mean ± SD (n = 3). Two-tailed unpaired t-test, statistical significance: *$p \leq 0.05$; **$p \leq 0.01$ *vs.* glass.

Hemolysis was analyzed to evaluate the potential of the material to induce red blood cell lysis, a critical parameter in hemocompatibility testing. Since significant hemolysis can lead to the release of intracellular components and subsequent

adverse systemic effects, it serves as an important indicator of the safety of blood-material interactions. In our study, none of the tested PHC-based materials exhibited hemolytic activity (0.16–0.5% hemolysis), confirming their excellent compatibility with blood, which showed a tendency to increase with increasing GSH concentration (Fig. 17C).

The plasma recalcification test (PRT) measured the prolongation of clotting time in recalcified plasma to assess the ability of the material to resist activation of the coagulation cascade that occurs when a biomaterial comes into contact with circulating blood.[71] Coagulation activation was inferred from an increase in plasma turbidity on the material surfaces, using a glass surface as a positive reference. The PRT for the glass surface was 11.42 ± 0.59 minutes, while the clotting time on the tested PHC-based materials was significantly prolonged up to 24.7 ± 3.6 minutes (Fig. 17D). These results correlate well with SEM images (Fig. 16) and indicate that all materials effectively suppressed plasma activation, regardless of the concentration of incorporated GSH.

Therefore, it can be concluded that all tested cPHC_2:3_10d materials showed good hemocompatibility, being non-thrombogenic, non-activating blood coagulation, non-hemolytic and non-inflammatory, although there was a slight upward trend in leukocyte activation with increasing GSH concentration in the sample. This is consistent with findings that GSH is not only an important antioxidant, but also an immunomodulatory agent necessary for the normal transduction of the activation signal from the outside to the inside of PMN leukocytes,[72] as well as for the physiological activation of lymphocytes and macrophages after contact with a pathogen, *e.g. Mycobacterium tuberculosis*.[73]

3. Conclusions and further perspectives

In this study, we present a previously unreported bifunctional modification of cross-linked poly(alkylene citrates) (cPACs) that highlights their potential applications in vascular tissue engineering. The introduction of the L-glutathione (GSH) molecules into the cross-linked polymer network resulted in two additional functionalities of cPACs: photoluminescence *via* the reaction of citric acid moieties with thermally hydrolyzed GSH residues and antioxidant properties due to the covalent and non-covalent bonding of remaining GSH molecules. The simultaneous modifications were confirmed *via* PL emission analyses and antioxidant activity measurements, which were further supported by dynamic mechanical and thermal characterization results. Conducted structural and physicochemical analyses revealed that the duration of cross-linking and the molar ratio of reactants significantly influence the fluorescent response and ROS-eliminating activity of cPACs. While materials obtained at a molar ratio of 1:1 (CA:diol) demonstrated marginally enhanced antioxidant properties compared to those obtained at a molar ratio of 2:3, they were deemed inadequate for cell viability studies due to the aforementioned higher acidity, which can impede their colonization with cells. Nevertheless, the results of the dynamic mechanical examination and elongation measurements indicated that the cross-linked material properties were not significantly affected by the addition of the modifier. It is noteworthy that the initial screening with human adipose tissue-derived stem cells (ASCs) indicated that cPOC-based materials were unsuitable for cell colonization due to their high acidity. Consequently, the cell culture test was continued with cPHC-based materials only. The cPHC, with all tested concentrations of GSH, proved to be suitable substrates for the adhesion of ASCs, fibroblasts (NHDFs), endothelial cells (HUVECs), and vascular smooth muscle cells (SMCs). In the presence of induced oxidative stress, ASCs and NHDFs exhibited a reduction in metabolic activity across all tested substrates. Conversely, HUVECs and SMCs demonstrated an increase or, at the very least, a maintenance of metabolic activity. GSH demonstrated a slight concentration-dependent protective effect on ASCs and NHDFs, but no effect on SMCs, and even a slight (though not statistically significant) adverse effect on HUVECs. Therefore, it is essential to consider the cell type-specific differences in the response to oxidative stress and the presence of antioxidants in the growth substrate when reconstructing irreversibly damaged blood vessels. In addition, a potential intrinsic antioxidant activity of cPAC materials, which could mask the antioxidant effect of GSH, should be considered. Nevertheless, the presented results highlight the significance of incorporating GSH into cPAC materials to elicit a protective effect on cell growth. Finally, in light of the aforementioned conclusions, it can be stated that the introduction of GSH *via* a single-step bifunctional modification to cross-linked poly(alkylene citrates) has resulted in a notable enhancement of their biocompatibility and the acquisition of photoluminescent properties. Both of these attributes hold significant value in the context of the further development of these materials for potential application in soft tissue engineering. The good hemocompatibility of the material demonstrated in our study makes it particularly promising for vascular tissue engineering.

4. Experimental

4.1. Reagents and cells

The following reagents were used for the preparation of the cPAC-based materials: anhydrous citric acid (CA) (Alfa Aesar); 1,6-hexanediol (HEX) (TCI); 1,8-octanediol (OCT) (Angene); L-glutathione (GSH) (Fluorochem); methanol (Avantor); ethanol (Avantor); dimethyl sulfoxide-d6 (Aldrich); 2,2-diphenyl-1-picrylhydrazyl (Aldrich). All chemicals and solvents were analytical grade and were used as received. Deionized water used throughout the experiments was purified by a Purix water purification system.

The following cell types, media, and other laboratory supplies were used to evaluate the biocompatibility and antioxidant activity of the materials: laboratory isolated adipose tissue-derived stem cells (ASCs; Institute of Physiology of the Czech Academy of Sciences, Prague, Czech Republic) and

commercially available normal neonatal human dermal fibroblasts (NHDFs; Lonza, Basel, Switzerland, Cat. No. CC-2509), human umbilical vein endothelial cells (HUVECs; Lonza, Basel, Switzerland, Cat. No. C2517A), and human umbilical artery smooth muscle cells (SMCs; PromoCell, Heidelberg, Germany, Cat. No. C-12500); Dulbecco's modified Eagle medium (DMEM, Sigma-Aldrich, Merck, Darmstadt, Germany, Cat. No. D5648), fetal bovine serum (FBS; Thermo Fisher Scientific, Waltham, MA, USA, Cat. No. 10270-106), gentamicin (Lek Pharmaceuticals, Ljubljana, Slovenia), FGF-2 (GenScript, Piscataway, NJ, USA, Cat. No. Z03116-1), EGM2 basal medium (PromoCell, Heidelberg, Germany, Cat. No. C-22211) with growth medium supplement pack 2 (PromoCell, Heidelberg, Germany, Cat. No. C-39211), SMCGM-2 basal medium (PromoCell, Heidelberg, Germany, Cat. No. C-22262) with growth medium supplement pack-2 (PromoCell, Heidelberg, Germany, Cat. No. C-39262), antibiotics & antimycotics (Sigma-Aldrich, Merck, Darmstadt, Germany, 1 : 100; Cat. No. A5955-100ML), 24-well tissue culture flat bottom plates (ThermoFisher Scientific, Waltham, MA, USA, Cat. No. 142475), 48-well polystyrene cell culture plates (TPP, Trasadingen, Switzerland, Cat. No. 92048), menadione (Sigma-Aldrich, Merck, Darmstadt, Germany, Cat. No. M5625), resazurin (Sigma-Aldrich, Merck, Darmstadt, Germany, Cat. No. R7017), CellTiter-Glo® luminescent cell viability assay (Promega, Madison, WI, USA, Cat. No. G9241), white opaque Nunc™ MicroWell™ 96-Well, nunclon delta-treated, flat-bottom microplate (Thermo Fisher Scientific, Waltham, MA, USA, Cat. No. 136101), ROS Detection Assay Kit (DFCDA/H_2DCFDA; Canvax Reagents, Valladolid, Spain; Cat. No. CA093), black 96-well glass-bottom plates with lids (Cellvis, Mountain View, CA, USA; Cat. No. P96-1.5H-N), E-plate view 96 PET, (ACEA Biosciences, San Diego, CA, USA, Cat. No. 300600910).

4.2. Synthesis of materials

4.2.1. Prepolymer synthesis. The prepolymer synthesis protocol has been described elsewhere.[24] Briefly, citric acid and a specific diol were mixed in glass vials at molar ratios of 1 : 1 and 2 : 3 (Table 2). The reactants were then heated at 140 °C for 40 minutes under stirring (100 rpm) (each reaction vial containing reactants was weighed before and after synthesis). The resulting reaction mixtures were dissolved in 40 mL of 96% ethanol, precipitated in 150 mL of deionized water, centrifuged (MPW-350, 5000 rpm, 10 min; each centrifuge tube was weighed before being filled with PAC suspension), and freeze dried (CHRIST Alpha 2-4 LDplus, 0.35 mbar, −85 °C). After lyophilization, the purified prepolymers (PHC_1 : 1, PHC_2 : 3, POC_1 : 1 and POC_2 : 3) were dissolved in ethanol to obtain 30% w/v solutions used for crosslinking.

Table 3 Indications and concentrations of GSH (G) solutions used to modify cPAC materials

Solution indication	Modifier concentration [mg mL^{-1}]
G0.4	50
G0.8	100
G1.6	150

4.2.2. Modification protocol and crosslinking process. Aqueous solutions of GSH at various concentrations were prepared to obtain modified cPAC materials (Table 3). Solutions were prepared by weighing appropriate amounts of GSH on an analytical balance, transferring them to volumetric flasks, adding water to the mark, and dissolving the contents in an ultrasonic bath. The resulting solutions were stored at 4 °C and used to prepare modified materials.

Modified materials were prepared in polypropylene molds. Initially, 2.5 mL of an aqueous GSH solution of the modifier at the appropriate concentration was added to the mold. Then 100 mL of a 30% ethanol solution of the respective prepolymer was poured in, stirred gently, and placed in a dryer for crosslinking (Fig. 18). The selected volumes of prepolymer and modifier solutions enabled achieving final modifier concentrations of 0.4, 0.8 and 1.6%, respectively, in the materials.

The post-polymerization process was carried out by casting 30% w/v prepolymer solutions onto polypropylene or polystyrene molds and curing for 4 or 10 days at 80 °C. During the first day, the samples were cured at atmospheric pressure, and during the remaining days at reduced pressure (200 mbar). As a result, control and modified crosslinked poly(1,6-hexamethylene citrate) (PHC) samples and poly(1,8-octamethylene citrate) (POC) samples were obtained (Table 4).

4.3. Materials characterization

4.3.1. ^{13}C MAS NMR analyses of cPACs. All ^{13}C MAS NMR analyses were carried out at the NMR laboratory of the Institute of Macromolecular Chemistry of the Czech Academy of Sciences, Prague. The material samples were analyzed using an Avance III HD 500 MHz spectrometer (Bruker, Germany) with the magic angle spinning (MAS) frequency for the sample at 15 kHz. The delay between consecutive scans was 15 seconds. The chemical shift scale on the ^{13}C NMR spectrum was calibrated using glycine as an external standard (176.03 ppm). To compensate for heating caused by the friction of the rotating samples, all NMR experiments were recorded under active cooling. The sample temperature was maintained at

Table 2 Weights of reagents used in the syntheses of the prepolymers and corresponding sample identifiers

PHC					POC				
Sample	CA [g]	Diol [g]	CA [mol]	Diol [mol]	Sample	CA [g]	Diol [g]	CA [mol]	Diol [mol]
PHC_1 : 1	12.38	7.62	0.065	0.065	POC_1 : 1	11.36	8.64	0.059	0.059
PHC_2 : 3	10.40	9.60	0.054	0.081	POC_2 : 3	9.34	10.66	0.049	0.073
PHC_1 : 2	8.97	11.03	0.047	0.093	POC_1 : 2	7.93	12.07	0.041	0.083

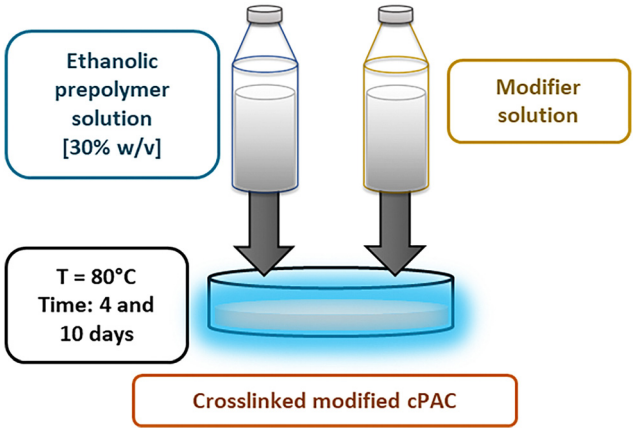

Fig. 18 Graphical illustration of cPACs materials modification.

25 °C, and the temperature calibration was performed on $Pb(NO_3)_2$ using the calibration procedure described in the literature.[74]

4.3.2. Spectroscopy analyses of cPACs. Photoluminescence emission measurement studies of the samples were performed using an RF-6000 spectrofluorophotometer (Shimadzu, Japan) controlled by LabSolutionsRF software, equipped with a fixed mount adapter for solid samples. A circular section with a diameter of 12 mm was punched from each material. Emission spectra were recorded in the wavelength range of 400–600 nm with an excitation wavelength of 355 nm. Both, the emission and excitation slits were set to 5 nm. For the acquisition of 3D spectra, the excitation wavelength range was set to 200–400 nm, the emission wavelength range to 300–600 nm, and the slit widths for both emission and excitation were set to 3 nm.

4.3.3. Antioxidant properties of cPACs. To evaluate the antioxidant properties of the obtained materials, a DPPH radical scavenging assay was performed. A DPPH solution was prepared by dissolving 15.8 mg of DPPH in 100 mL of 99.5% methanol. Three 12 mm disk-shaped samples were punched from each material using a punch and placed in a transparent 24-well plate (Thermo Fisher Scientific, Waltham, MA, USA; Cat. No. 142475). Samples of unmodified materials served as blanks. Each sample was treated with 500 μL of DPPH solution and 100 μL of methanol and incubated in the dark for 2 hours. After incubation, 200 μL of the solution from each well was transferred to a 96-well plate (VWR, Radnor, PA, USA), and the absorbance was measured at 517 nm using an Infinite 200 PRO plate reader (Tecan, Männerdorf, Switzerland).

4.3.4. Mechanical characterization of cPACs. Elongation and tensile strength measurements were performed using a Zwick Model 1445 testing machine (Zwick Roell, Ulm, Germany) in accordance with the ASTM D412 standard. Samples (five per material) were cut from larger sheets of crosslinked materials using an appropriate punch, cleaned with methanol, and their dimensions were measured with a caliper prior to testing. The elongation rate was set to 500 mm min^{-1}, based on similar protocols reported in the literature.[23]

4.3.5. Hardness measurements of cPACs. The hardness of the crosslinked polymers was measured according to the ASTM D2240 type A scale for elastomers and rubbers using a Shore A durometer (INSIZE INC., Loganville, GA, USA). Measurements were performed by pressing the flat foot of the durometer into the material, with the hardness value recorded after 15 seconds. Both sides of each specimen (top and bottom) were tested in duplicate at different locations.

4.3.6. Dynamic-mechanical and thermal analysis of cPACs. Dynamic-mechanical and thermal analysis (DMTA) of the crosslinked polymers was performed on ARES-G2 rheometer (TA Instruments, USA). The temperature dependence of complex shear modulus (G^*) was determined on rectangular samples (10 mm × 5 mm × 1 mm) using oscillatory shear deformation (0.1% strain) at 1 Hz frequency from −50 to 150 °C at a temperature heating rate of 3 °C min^{-1}. The main transition temperature (T_α) was determined as the $\tan\delta$ (loss tangent) peak maximum. Storage modulus at rubber plateau (G'_R) was determined at $T = T_\alpha + 50$ K. From the G'_R values, the effective cross-link density (ν_e) was then calculated using the following equation:

$$\nu_e = G'_R/[R(T_\alpha + 50)]$$

where R is the universal gas constant.

4.4. Cell culture experiments

4.4.1. Cytocompatibility of GSH-enriched cPACs. The cPOC_2:3_10d and cPHC_2:3_10d materials without or with

Table 4 Overview of samples of control and modified cPAC materials obtained from the reactions performed

	PHC		POC	
Modifier	1:1	2:3	1:1	2:3
Crosslinking time 4 days				
None	cPHC_1:1_4d_C	cPHC_2:3_4d_C	cPOC_1:1_4d_C	cPOC_2:3_4d_C
G0.4	cPHC_1:1_4d_G0.4	cPHC_2:3_4d_G0.4	cPOC_1:1_4d_G0.4	cPOC_2:3_4d_G0.4
G0.8	cPHC_1:1_4d_G0.8	cPHC_2:3_4d_G0.8	cPOC_1:1_4d_G0.8	cPOC_2:3_4d_G0.8
G1.6	cPHC_1:1_4d_G1.6	cPHC_2:3_4d_G1.6	cPOC_1:1_4d_G1.6	cPOC_2:3_4d_G1.6
Crosslinking time 10 days				
None	cPHC_1:1_10d_C	cPHC_2:3_10d_C	cPOC_1:1_10d_C	cPOC_2:3_10d_C
G0.4	cPHC_1:1_10d_G0.4	cPHC_2:3_10d_G0.4	cPOC_1:1_10d_G0.4	cPOC_2:3_10d_G0.4
G0.8	cPHC_1:1_10d_G0.8	cPHC_2:3_10d_G0.8	cPOC_1:1_10d_G0.8	cPOC_2:3_10d_G0.8
G1.6	cPHC_1:1_10d_G1.6	cPHC_2:3_10d_G1.6	cPOC_1:1_10d_G1.6	cPOC_2:3_10d_G1.6

GSH (concentrations of 0.4, 0.8, and 1.6% w/w) were placed in 24-well tissue culture flat-bottom plates (Thermo Fisher Scientific, Waltham, MA, USA, Cat. No. 142475). Prior to cell seeding, samples were disinfected with 70% ethanol (1 hour; room temperature) followed by UV irradiation (20 minutes; room temperature). Each material sample was then thoroughly washed (5 times in 3 days) with medium appropriate for the cell type seeded to reduce acidity caused by non-crosslinked citrate groups.

As an initial screening of the suitability of the aforementioned samples for cell colonization, adipose tissue-derived stem cells (ASCs) were used as a cell type considered suitable for blood vessel reconstruction. ASCs were isolated from a lipoaspirate obtained by liposuction of subcutaneous fat from the abdominal region of a healthy adult female (age 41 years). The isolation was performed in accordance with the tenets of the Declaration of Helsinki for human tissue experimentation and under the ethical approval of the Ethics Committee of the Na Bulovce Hospital in Prague, Czech Republic (June 11, 2019, further updated on March 15, 2022). Written informed consent was obtained from the patient prior to liposuction. The isolation of ASCs from the lipoaspirate was described in detail in our previous studies, along with flow cytometric characterization of the ASCs to confirm the presence of mesenchymal stem cells and the absence of other cell types.[24,48,53,64] The ASCs (passage 3) were then seeded on the materials at a density of 2.5×10^4 cells per sample (approximately 13 000 cells cm^{-2}) in Dulbecco's modified Eagle's medium (DMEM; Sigma-Aldrich, Merck, Darmstadt, Germany, Cat. No. D5648) supplemented with 10% fetal bovine serum (FBS; Thermo Fisher Scientific, Waltham, MA, USA, Cat. No. 10270-106), 40 μg mL^{-1} gentamicin (Lek Pharmaceuticals, Ljubljana, Slovenia) and 10 ng mL^{-1} FGF-2 (GenScript, Piscataway, NJ, USA, Cat. No. Z03116-1). ASCs were used for the initial screening of the suitability of cPOC_2 : 3_10d and cPHC_2 : 3_10d samples with different concentrations of GSH (0.0, 0.4, 0.8 and 1.6% w/w) for cell adhesion and growth. Since the advantage of the tested materials is their transparency, cell morphology in native cultures was evaluated using an inverted Olympus IX71 microscope (Fig. 8).

After selecting cPHC_2 : 3_10d for further cell experiments, ASCs were used to compare cell morphology and growth on this material with increasing concentrations of GSH (0.0, 0.4, 0.8, and 1.6% w/w) and on control TCPS (Fig. 9). In the next experiment, cell morphology and growth on cPHC_2 : 3_10d with increasing GSH concentrations was compared in ASCs and other cell types relevant for vascular tissue engineering, such as fibroblasts, endothelial cells and smooth muscle cells present in the tunica adventitia, tunica intima and tunica media of the vessel wall, respectively (Fig. 10). Thus, in addition to ASCs, the following cell models were used:

- Normal human neonatal dermal fibroblasts (NHDFs), purchased from Lonza (Basel, Switzerland, Cat. No. CC-2509) and seeded at a density of 2.0×10^4 cells per sample (approximately 10 000 cells cm^{-2}) in DMEM containing 10% FBS and gentamicin (40 μg mL^{-1});
- Human umbilical vein endothelial cells (HUVECs), purchased from Lonza (Basel, Switzerland, Cat. No. C2517A), were seeded at a density of 2.0×10^4 cells per sample (approximately 10 000 cells cm^{-2}) in EGM2 basal medium (PromoCell, Heidelberg, Germany, Cat. No. C-22211) supplemented with hydrocortisone, heparin, ascorbic acid and 2% FBS from the growth medium supplement package 2 (PromoCell, Heidelberg, Germany, Cat. No. C-39211) and antibiotic & antimycotics (AbAm; Sigma-Aldrich, Merck, Darmstadt, Germany, 1 : 100; Cat. No. A5955-100ML); and
- Human umbilical artery smooth muscle cells (SMCs), purchased from PromoCell (Heidelberg, Germany, Cat. No. C-12500) and seeded at a density of 3.0×10^4 cells per sample (approximately 15 500 cells cm^{-2}) in SMCGM-2 basal medium (PromoCell, Heidelberg, Germany, Cat. No. C-22262) supplemented with epidermal growth factor, basic fibroblast growth factor, insulin and 5% FBS in the growth medium 2 supplement pack (PromoCell, Heidelberg, Germany, Cat. No. C-39262) and with AbAm (Sigma-Aldrich, Merck, Darmstadt, Germany, 1 : 100; Cat. No. A5955-100ML).

On day 3 after seeding, ASCs, NHDFs, HUVECs, and SMCs on the tested materials were stained with hematoxylin and eosin and examined under an Olympus IX71 microscope in bright field mode (Fig. 9 and 10).

The reason for seeding ASCs, NHDFs, HUVECs and SMCs at different population densities was due to their different sizes and growth rates. It was necessary for all cell types to reach similar population densities (*i.e.* 80% confluence) in all samples tested on day 3 after seeding, when cell metabolic activity under oxidative stress was assessed.

4.4.2. Oxidative stress of cells on GSH-enriched cPACs. Oxidative stress of the cells was induced by the addition of menadione to the culture medium. First, the most appropriate concentration of menadione was determined in three-day cultures of ASCs on TCPS and cPHC_2 : 3_10d samples containing 0.0, 0.4, 0.8, and 1.6% w/w GSH. Menadione (Sigma-Aldrich, Merck, Darmstadt, Germany, Cat. No. M5625) was used at concentrations ranging from 50 μM to 500 mM. Cells were preincubated with menadione for 1 or 2 hours and then the metabolic activity of the cells was evaluated by a resazurin assay (Fig. 11). This assay is based on a colorimetric reduction reaction of resazurin (blue; also called Alamar blue) to resorufin (pink; measured fluorescence intensity at 590 nm emission, excited at 530 nm). ASCs were incubated with 40 nM resazurin for 3 hours in medium without phenol red. For samples preincubated with menadione, the same concentration of menadione was also added to the resazurin-containing medium to prevent cell recovery from menadione pretreatment, which was often observed in our preliminary experiments. Thus, cells were incubated in menadione for a total of 5 and 6 hours. Native cultures of cells preincubated with menadione for 1 and 2 hours were also observed under an inverted Olympus IX71 microscope (Fig. 12).

For further experiments, the concentration of 500 μM was selected as the most appropriate concentration of menadione and was added to three-day cultures of ASCs, NHDFs, HUVECs,

and SMCs on TCPS and cPHC_2 : 3_10d samples with 0.0, 0.4, 0.8, and 1.6% w/w GSH. Prior to the addition of menadione, the basal metabolic activity of the cells was measured by incubating the cells with 40 nM resazurin for 3 hours. The medium was then replaced with fresh medium, and half of the samples monitored were exposed to menadione at a concentration of 500 μM for 3 hours. In the next step, the culture medium was changed to the medium containing resazurin for all samples tested, and the cells were incubated for another 3 hours. For samples preincubated with 500 μM menadione, the same concentration of menadione was also added to the resazurin medium (to prevent recovery of cells from the menadione pre-treatment). Thus, half of the samples were incubated with menadione for 6 hours (*i.e.* 3 hours pre-incubation in medium without resazurin and 3 hours incubation in medium with resazurin) and the other half were incubated in menadione-free medium for 6 hours.

As control samples, all investigated sample groups (TCPS and cPHC_2 : 3_10d with 0.0, 0.4, 0.8 and 1.6% w/w GSH) that were not seeded with cells underwent the same procedure as the cell-seeded samples described above. The reason for this approach was to monitor any non-specific reaction of resazurin with the material or with menadione. The fluorescence intensity of the non-cell-seeded samples was then subtracted (as 'background') from the fluorescence intensity of the corresponding cell-seeded samples. Finally, the fluorescence intensity of the cells after incubation with menadione was divided by the fluorescence intensity of the corresponding cells before incubation with menadione, and the resulting ratios were plotted on a graph (Fig. 13). A ratio of 1 indicates that the metabolic activity of the cells after incubation with menadione was the same as before incubation, a ratio greater than 1 indicates that this metabolic activity was higher, and a ratio less than 1 indicates a decrease in the metabolic activity of the cells after incubation with menadione.

For each group of samples, 3–6 measurements of metabolic activity were performed (usually 3 measurements for samples without menadione and 6 measurements for samples with menadione).

Further analysis of cell viability on the tested materials under menadione stress was performed using the CellTiter-Glo® luminescent cell viability assay (Promega, Madison, WI, USA; Cat. No. G9241) according to the manufacturer's protocol (Fig. 14). Briefly, ASCs were seeded on cPHC_2 : 3_10d materials containing 0, 0.4, 0.8, or 1.6% w/w GSH in 96-well polystyrene (PS) cell culture plates (TPP, Trasadingen, Switzerland) and in pure PS wells at a concentration of 10 000 cells per well in 100 μL phenol red-free DMEM supplemented with 10% FBS (Thermo Fisher Scientific, Waltham, MA, USA, Cat. No. 10270-106), 40 μg mL^{-1} gentamicin (Lek Pharmaceuticals, Ljubljana, Slovenia) and 10 ng mL^{-1} FGF-2 (GenScript, Piscataway, NJ, USA, Cat. No. Z03116-1). After 48 hours of incubation (37 °C, humidified air atmosphere with 5% CO_2), the medium was replaced with 100 μL of the same medium and supplemented with menadione to a final concentration of 100 μM. Control cells were left without menadione. After 2 hours, 100 μL of CellTiter-Glo® reagent was added to both menadione-exposed and menadione-free cells, and incubated for 2 minutes on an orbital shaker to achieve cell lysis. The resulting solutions containing cell lysates were then pipetted into white opaque Nunclon™ delta surface 96-well polystyrene plates (Thermo Fisher Scientific, Waltham, MA, USA, Cat. No. 136101) and the luminescence of oxyluciferin (*i.e.* the luminescent product of Ultra-Glo™ luciferase, which uses mitochondrial ATP from living cells to convert D-luciferin) was measured using a Cytation 3 reader (BioTek, Winooski, VT, USA; excitation: 560 nm, emission: full light).

The generation of reactive oxygen species (ROS) in ASCs exposed to menadione was evaluated using the ROS Detection Assay Kit (DFCDA/H_2DCFDA; Canvax Reagents, Valladolid, Spain; Cat. No. CA093; Fig. 15). Cells were seeded into black 96-well glass-bottomed plates with lids (Cellvis, Mountain View, CA, USA; Cat. No. P96-1.5H-N). Each well contained 12 500 cells in 200 μL of control DMEM supplemented as described above or extracts of the tested materials.

To prepare the extracts, the materials (circles 1 cm in diameter) were placed in 48-well polystyrene cell culture plates (TPP, Trasadingen, Switzerland) and thoroughly washed as before cell culture, *i.e.*, 5 times in 3 days with the medium used for the cultivation of ASCs, *i.e.*, DMEM with 10% FBS, 40 μg mL^{-1} gentamicin and 10 ng mL^{-1} FGF-2 (1 mL per well for each medium change), to reduce the acidity of the materials caused by non-crosslinked citrate groups. After washing, 1 mL of the same medium was added to the materials for 24 hours and then discarded. Fresh medium (1 mL per well) was added to the wells and the materials were extracted for 48 hours. From each group of materials, 12 samples were used and 12 mL of the medium were prepared.

One day after seeding, the extracts or the control medium were replaced with 100 μL of fresh ones, either without menadione or with 500 μM menadione. After 2 hours of incubation, 100 μL of 2′,7′-dichlorodihydrofluorescein diacetate (H_2DCFDA) working solution, prepared in the extracts or control DMEM, was added to each well to a final H_2DCFDA concentration of 30 μM, and the cells were incubated for 1 hour. Fluorescence of 2′,7′-dichlorodihydrofluorescein, generated in the presence of ROS, was then detected from the bottom of the plates using a Synergy H1M Reader (BioTek, Winooski, VT, USA; excitation: 485 nm, emission: 535 nm).

The material extracts were also used to monitor the proliferation of ASCs exposed to menadione using the xCELLigence real-time cell analyzer (Agilent Technologies, Santa Clara, CA, USA; Fig. S8 in the ESI†). This monitoring requires direct cell attachment to the bottom of E-plate wells (E-plate view 96 PET, Cat. No. 300600910, ACEA Biosciences, San Diego, CA, USA) with interdigitated gold microelectrodes. Each well contained 5000 ASCs in 100 μL of standard DMEM medium supplemented with 10% FBS, 40 μg mL^{-1} gentamicin, and 10 ng mL^{-1} FGF-2, as described above. The cells were allowed to adhere and spread for 1 day and then the medium was replaced with extracts of the tested materials (100 μL per well). Standard DMEM culture medium with appropriate supplements was used for control cells. After another 1 day, 5 μL of the extracts

or of control medium, either with menadione (final concentration of 500 μM or 15 μM) or without menadione, was added to each well. Cells were then cultured for 1–3 days and the cell index was monitored every 30 minutes. Four wells were used per each experimental group.

4.4.3. Hemocompatibility of GSH-enriched cPACs. Fresh human whole blood was collected by venipuncture from healthy volunteers (n = 3) and anticoagulated either with heparin (final concentration 1 IU mL^{-1}) or citrate (3.2%). Citrated plasma was prepared by centrifuging the citrated blood at 3500g for 10 minutes. The resulting plasma was immediately frozen in liquid nitrogen and stored at −80 °C until further analysis. All blood samples were collected in accordance with the regulations of the Ethics Committee of the Institute of Hematology and Blood Transfusion, Prague, Czech Republic, and with the informed consent of the donor.

To evaluate hemocompatibility (Fig. 16 and 17), the cPHC-based materials were exposed to freshly drawn heparinized whole blood and incubated for 60 minutes at 37 °C with gentle shaking. After the incubation, the materials were used for scanning electron microscopy (SEM), while the blood was transferred to tubes containing citrate (3.2%) and centrifuged at 3500g for 10 minutes. The obtained plasma was immediately frozen in liquid nitrogen and stored at −80 °C for subsequent analyses of inflammatory markers related to leukocyte activation, *i.e.* polymorphonuclear (PMN) elastase and complement activation (SC5b-9). Enzyme-linked immunosorbent assays (ELISAs) were performed according to the manufacturer's instructions to measure specific biomarkers of inflammation (PMN elastase/α1-PI complex, Demeditec Diagnostics GmbH, Kiel, Germany) and complement activation (SC5b-9, Quidel, San Diego, CA, USA).

After the incubation of the samples with fresh whole blood (60 minutes at 37 °C, as described above), the samples were thoroughly washed with phosphate-buffered saline (PBS), cross-linked with 0.5% glutaraldehyde for 2 hours at room temperature, washed again, and dehydrated by successive incubation with aqueous solutions containing gradually increasing concentrations of ethanol. The dehydrated surfaces were platinum sputtered and observed by SEM using a VEGA Plus TS 5135 microscope (Tescan, Brno, Czech Republic).

Hemolysis was evaluated after contact of isolated erythrocytes with the samples. First, freshly drawn human blood was centrifuged at 1500g for 10 minutes to separate the erythrocytes from the plasma. The plasma and buffy coat were removed, and PBS was added to the erythrocytes and gently mixed. The erythrocytes were centrifuged at 1500g for 10 minutes, and the supernatant was removed and replaced with fresh PBS. The washing step was repeated three times. Finally, a 2% solution of erythrocytes in saline (0.9%) was prepared, added to the tested material samples, and incubated for 4 hours at 37 °C with gentle shaking. After incubation, the erythrocyte solution was collected and centrifuged at 1500g for 10 min, and the absorbance of the supernatant was measured at 540 nm. As a positive control, erythrocytes were lysed in deionized water (100% hemolysis).

The tested materials were placed in 24-well tissue culture flat-bottom plates (Thermo Fisher Scientific, Waltham, MA, USA, Cat. No. 142475) and incubated with citrated human blood plasma freshly recalcified with $CaCl_2$ (0.02 M final concentration). The light transmission through the PHC material and the layer of recalcified plasma was then measured at 350 nm every 20 seconds for 1 hour using a microplate reader (Epoch, Biotek, Winooski, VT, USA). The transmission decreased due to the turbidity of the plasma clot formed on the coated surface. The plasma recalcification time (PRT) was defined for our experiments as the time from the addition of freshly recalcified plasma to a well to the half-minimum in the S-shaped transmission *versus* time curve. A glass surface (microscopic glass coverslips, P-LAB a.s., Prague, Czech Republic, Cat. No. H101112.1) was used as a positive control.

Data availability

The data supporting this article have been included as part of the ESI.†

Conflicts of interest

There are no conflicts to declare.

Acknowledgements

This research was financed by the Polish National Science Centre for years 2018–2021; SONATINA No. UMO-2018/28/C/ST5/00461, for years 2022–2026 PRELUDIUM No. UMO-2021/41/N/ST4/03362 and by the Project No. CZ.02.01.01/00/22_008/0004562 of the Ministry of Education, Youth and Sports of the Czech Republic, co-funded by the European Union. Further support was provided by the Praemium Academiae grant (No. AP 2202) of the Czech Academy of Sciences. Robin Healey (Czech Technical University in Prague, Czech Republic) is gratefully acknowledged for the language revision of the manuscript.

References

1 G. D. Flora, *et al.*, A Brief Review of Cardiovascular Diseases, Associated Risk Factors and Current Treatment Regimes, *Curr. Pharm. Des.*, 2019, **25**(38), 4063, DOI: 10.2174/1381612825666190925163827.
2 H. Thomas, *et al.*, Global Atlas of Cardiovascular Disease 2000–2016: The Path to Prevention and Control, *Global Heart*, 2018, **13**(3), 143, DOI: 10.1016/j.gheart.2018.09.511.
3 H. Tunstall-Pedoe, Cardiovascular risk and risk scores: ASSIGN, Framingham, QRISK and others: How to choose, *Heart*, 2011, **97**(6), 442, DOI: 10.1136/hrt.2010.214858.
4 J. Gutierrez, *et al.*, Statin Therapy in the Prevention of Recurrent Cardiovascular Events, *Arch. Intern. Med.*, 2012, **172**(12), 909, DOI: 10.1001/archinternmed.2012.2145.

5 G. N. Kouvelos, *et al.*, Balloon Angioplasty Versus Stenting for the Treatment of Failing Arteriovenous Grafts: A Meta-Analysis, *Eur. J. Vasc. Endovasc. Surg.*, 2018, **55**(2), 249, DOI: 10.1016/j.ejvs.2017.11.011.
6 J. Chlupác, *et al.*, Blood vessel replacement: 50 years of development and tissue engineering paradigms in vascular surgery, *Physiol. Res.*, 2009, **58**(SUPPL.2), 119, DOI: 10.33549/physiolres.931918.
7 H. H. G. Song, *et al.*, Vascular Tissue Engineering: Progress, Challenges, and Clinical Promise, *Cell Stem Cell*, 2018, **22**(3), 340, DOI: 10.1016/j.stem.2018.02.009.
8 T. Sultana, *et al.*, Preparation and characterization of polycaprolactone–polyethylene glycol methyl ether and polycaprolactone–chitosan electrospun mats potential for vascular tissue engineering, *J. Biomater. Appl.*, 2017, **32**(5), 648, DOI: 10.1177/0885328217733849.
9 C. Zhu, *et al.*, Initial investigation of novel human-like collagen/chitosan scaffold for vascular tissue engineering, *J. Biomed. Mater. Res., Part A*, 2009, **89**(3), 829, DOI: 10.1002/jbm.a.32256.
10 A. Yin, *et al.*, Performance of PEGylated chitosan and poly (L-lactic acid-*co*-ε-caprolactone) bilayer vascular grafts in a canine femoral artery model, *Colloids Surf., B*, 2020, **188**, 110806, DOI: 10.1016/j.colsurfb.2020.110806.
11 D. Zhang, *et al.*, Dealing with the Foreign-Body Response to Implanted Biomaterials: Strategies and Applications of New Materials, *Adv. Funct. Mater.*, 2021, **31**(6), 2007226, DOI: 10.1002/adfm.202007226.
12 J. M. Anderson, Biological responses to materials, *Annu. Rev. Mater. Sci.*, 2001, **31**, 81, DOI: 10.1146/annurev.matsci.31.1.81.
13 J. M. Anderson, *et al.*, Foreign body reaction to biomaterials, *Semin. Immunol.*, 2008, **20**(2), 86, DOI: 10.1016/j.smim.2007.11.004.
14 M. Hedayati, *et al.*, The quest for blood-compatible materials: Recent advances and future technologies, *Mater. Sci. Eng., R*, 2019, **138**, 118, DOI: 10.1016/j.mser.2019.06.002.
15 L. Yu, *et al.*, Coating small-diameter ePTFE vascular grafts with tunable poly(diol- co -citrate- co -ascorbate) elastomers to reduce neointimal hyperplasia, *Biomater. Sci.*, 2021, **9**(15), 5160, DOI: 10.1039/D1BM00101A.
16 T. Fukayama, *et al.*, Effect of fibroin sponge coating on in vivo performance of knitted silk small diameter vascular grafts, *Organogenesis*, 2015, **11**(3), 137, DOI: 10.1080/15476278.2015.1093268.
17 W. Jia, *et al.*, Design and comprehensive assessment of a biomimetic tri-layer tubular scaffold *via* biodegradable polymers for vascular tissue engineering applications, *Mater. Sci. Eng., C*, 2020, **110**, 110717, DOI: 10.1016/j.msec.2020.110717.
18 S. G. Wise, *et al.*, A multilayered synthetic human elastin/polycaprolactone hybrid vascular graft with tailored mechanical properties, *Acta Biomater.*, 2011, **7**(1), 295, DOI: 10.1016/j.actbio.2010.07.022.
19 U. Bertram, *et al.*, Vascular Tissue Engineering: Effects of Integrating Collagen into a PCL Based Nanofiber Material, *BioMed Res. Int.*, 2017, **2017**, 1, DOI: 10.1155/2017/9616939.
20 N. Wang, *et al.*, *In vitro* evaluation of essential mechanical properties and cell behaviors of a novel polylactic-*co*-glycolic acid (PLGA)-based tubular scaffold for small-diameter vascular tissue Engineering, *Polymers*, 2017, **9**(8), 318, DOI: 10.3390/polym9080318.
21 D. G. Seifu, *et al.*, Small-diameter vascular tissue engineering, *Nat. Rev. Cardiol.*, 2013, **10**(7), 410, DOI: 10.1038/nrcardio.2013.77.
22 J. Yang, *et al.*, Novel Citric Acid-Based Biodegradable Elastomers for Tissue Engineering, *Adv. Mater.*, 2004, **16**(6), 511, DOI: 10.1002/adma.200306264.
23 J. Yang, *et al.*, Synthesis and evaluation of poly(diol citrate) biodegradable elastomers, *Biomaterials*, 2006, **27**(9), 1889, DOI: 10.1016/j.biomaterials.2005.05.106.
24 F. Koper, *et al.*, Advancements in structure–property correlation studies of cross-linked citric acid-based elastomers from the perspective of medical application, *J. Mater. Chem. B*, 2021, **9**(32), 6425, DOI: 10.1039/D1TB01078F.
25 D. Motlagh, *et al.*, Hemocompatibility evaluation of poly(diol citrate) *in vitro* for vascular tissue engineering, *J. Biomed. Mater. Res., Part A*, 2007, **82**(4), 907, DOI: 10.1002/jbm.a.31211.
26 D. Gyawali, *et al.*, Citric acid-derived *in situ* crosslinkable biodegradable polymers for cell delivery, *Biomaterials*, 2010, **31**(34), 9092, DOI: 10.1016/J.BIOMATERIALS.2010.08.022.
27 C. Ma, *et al.*, *In vitro* cytocompatibility evaluation of poly(octamethylene citrate) monomers toward their use in orthopedic regenerative engineering, *Bioact. Mater.*, 2018, **3**(1), 19, DOI: 10.1016/j.bioactmat.2018.01.002.
28 H. Qiu, *et al.*, A citric acid-based hydroxyapatite composite for orthopedic implants, *Biomaterials*, 2006, **27**(34), 5845, DOI: 10.1016/j.biomaterials.2006.07.042.
29 E. J. Chung, *et al.*, Low-pressure foaming: A novel method for the fabrication of porous scaffolds for tissue engineering, *Tissue Eng., Part C*, 2012, **18**(2), 113, DOI: 10.1089/ten.tec.2011.0289.
30 N. Asadi, *et al.*, Nanocomposite hydrogels for cartilage tissue engineering: a review, *Artif. Cells, Nanomed., Biotechnol.*, 2018, **46**(3), 465, DOI: 10.1080/21691401.2017.1345924.
31 J. Yang, *et al.*, Modulating expanded polytetrafluoroethylene vascular graft host response *via* citric acid-based biodegradable elastomers, *Adv. Mater.*, 2006, **18**(12), 1493, DOI: 10.1002/adma.200600230.
32 R. McCabe, *et al.*, Fully Biodegradable Elastomer-Based Device for Oral Macromolecule Delivery, *ACS Appl. Bio Mater.*, 2024, **7**(6), 3777, DOI: 10.1021/acsabm.4c00147.
33 B. L. Turner, *et al.*, Biodegradable elastomeric circuit boards from citric acid-based polyesters, *npj Flexible Electron.*, 2023, **7**(1), 1, DOI: 10.1038/s41528-023-00258-z.
34 L. V. Thomas, *et al.*, A biodegradable and biocompatible PVA–citric acid polyester with potential applications as matrix for vascular tissue engineering, *J. Mater. Sci.:Mater. Med.*, 2009, **20**(S1), 259, DOI: 10.1007/s10856-008-3599-7.
35 B. M. Szydlowska, *et al.*, Polydiolcitrate–MoS 2 Composite for 3D Printing Radio-Opaque, Bioresorbable Vascular Scaffolds, *ACS Appl. Mater. Interfaces*, 2024, **16**(34), 45422, DOI: 10.1021/acsami.4c07364.

36 A. Khan, *et al.*, Highly Elastic, Biodegradable Polyester-Based Citrate Rubber for 3D Printing in Regenerative Engineering, *ACS Biomater. Sci. Eng.*, 2025, **11**(3), 1571, DOI: **10.1021/acsbiomaterials.4c01486**.

37 F. Li, *et al.*, Injectable Hydrogels for Vascular Tissue Engineering, *Methods in Molecular Biology*, Humana, New York, NY, 2022, p. 165, DOI: **10.1007/978-1-0716-1708-3_14**.

38 H. Zhao, *et al.*, Biodegradable nitric oxide-releasing poly(diol citrate) elastomers, *J. Biomed. Mater. Res., Part A*, 2010, **93**(1), 356, DOI: **10.1002/jbm.a.32536**.

39 I. Djordjevic, *et al.*, Poly[octanediol-*co*-(citric acid)-*co*-(sebacic acid)] elastomers: Novel bio-elastomers for tissue engineering, *Polym. Int.*, 2011, **60**(3), 333, DOI: **10.1002/pi.2996**.

40 H. Savoji, *et al.*, 3D Printing of Vascular Tubes Using Bioelastomer Prepolymers by Freeform Reversible Embedding, *ACS Biomater. Sci. Eng.*, 2020, **6**(3), 1333, DOI: **10.1021/acsbiomaterials.9b00676**.

41 F. Zou, *et al.*, Elastic, hydrophilic and biodegradable poly (1, 8-octanediol-*co*-citric acid)/polylactic acid nanofibrous membranes for potential wound dressing applications, *Polym. Degrad. Stab.*, 2019, **166**, 163, DOI: **10.1016/j.polymdegradstab.2019.05.024**.

42 D. Shan, *et al.*, Citrate-Based Fluorescent Biomaterials, *Adv. Healthcare Mater.*, 2018, **7**(18), 1800532, DOI: **10.1002/adhm.201800532**.

43 W. Kasprzyk, *et al.*, *Luminescence phenomena of biodegradable photoluminescent poly(diol citrates) Supplementary information*, 2013.

44 R. van Lith, *et al.*, Engineering biodegradable polyester elastomers with antioxidant properties to attenuate oxidative stress in tissues, *Biomaterials*, 2014, **35**(28), 8113, DOI: **10.1016/j.biomaterials.2014.06.004**.

45 H. Ben Yahia, *et al.*, Crystal growth, single crystal structure, and biological activity of thiazolo-pyridine dicarboxylic acid derivatives, *ACS Omega*, 2020, **5**(43), 27756, DOI: **10.1021/acsomega.0c01769**.

46 W. Kasprzyk, *et al.*, Novel efficient fluorophores synthesized from citric acid, *RSC Adv.*, 2015, **5**(44), 34795, DOI: **10.1039/C5RA03226A**.

47 W. Kasprzyk, *et al.*, Fluorescence assay for the determination of glutathione based on a ring-fused 2-pyridone derivative in dietary supplements, *Analyst*, 2021, **146**(6), 1897, DOI: **10.1039/D0AN02245D**.

48 A. Flis, *et al.*, Poly(octamethylene citrate) Modified with Glutathione as a Promising Material for Vascular Tissue Engineering, *Polymers*, 2023, **15**(5), 1322, DOI: **10.3390/polym15051322**.

49 K. Kwiecień, *et al.*, Degradation studies of poly(diol citrates) for vascular tissue engineering purposes, *Eng. Biomater.*, 2020, **65**(158), 65.

50 L. Flohé, The fairytale of the GSSG/GSH redox potential, *Biochim. Biophys. Acta, Gen. Subj.*, 2013, **1830**(5), 3139, DOI: **10.1016/j.bbagen.2012.10.020**.

51 S. C. Lu, Glutathione synthesis, *Biochim. Biophys. Acta, Gen. Subj.*, 2013, **1830**(5), 3143, DOI: **10.1016/j.bbagen.2012.09.008**.

52 D. A. Averill-Bates, The antioxidant glutathione, *Vitamins and Hormones*, Academic Press, 2023, p. 109, DOI: **10.1016/bs.vh.2022.09.002**.

53 E. Filova, *et al.*, Adipose-Derived Stem Cells in Reinforced Collagen Gel: A Comparison between Two Approaches to Differentiation towards Smooth Muscle Cells, *Int. J. Mol. Sci.*, 2023, **24**(6), 5692, DOI: **10.3390/ijms24065692**.

54 G. Loor, *et al.*, Menadione triggers cell death through ROS-dependent mechanisms involving PARP activation without requiring apoptosis, *Free Radical Biol. Med.*, 2010, **49**(12), 1925, DOI: **10.1016/j.freeradbiomed.2010.09.021**.

55 B. Jiang, *et al.*, Enabling non-invasive assessment of an engineered endothelium on ePTFE vascular grafts without increasing oxidative stress, *Biomaterials*, 2015, **69**, 110, DOI: **10.1016/j.biomaterials.2015.07.064**.

56 C. Xie, *et al.*, Bioactive Poly(octanediol-citrate-polyglycol) Accelerates Skin Regeneration through M2 Polarization Immunomodulating and Early Angiogenesis, *Adv. Healthcare Mater.*, 2022, **11**(10), 2101931, DOI: **10.1002/adhm.202101931**.

57 J. Yang, *et al.*, A Thermoresponsive Biodegradable Polymer with Intrinsic Antioxidant Properties, *Biomacromolecules*, 2014, **15**(11), 3942, DOI: **10.1021/bm5010004**.

58 R. Campagna, *et al.*, Nicotinamide N-methyltransferase in endothelium protects against oxidant stress-induced endothelial injury, *Biochim. Biophys. Acta, Mol. Cell Res.*, 2021, **1868**(10), 119082, DOI: **10.1016/j.bbamcr.2021.119082**.

59 K. R. Katikireddy, *et al.*, NQO1 downregulation potentiates menadione-induced endothelial-mesenchymal transition during rosette formation in Fuchs endothelial corneal dystrophy, *Free Radical Biol. Med.*, 2018, **116**, 19, DOI: **10.1016/j.freeradbiomed.2017.12.036**.

60 H. Cai, *et al.*, MnSOD marks cord blood late outgrowth endothelial cells and accompanies robust resistance to oxidative stress, *Biochem. Biophys. Res. Commun.*, 2006, **350**(2), 364, DOI: **10.1016/j.bbrc.2006.09.046**.

61 D. Burtenshaw, *et al.*, Reactive Oxygen Species (ROS), Intimal Thickening, and Subclinical Atherosclerotic Disease, *Front. Cardiovasc. Med.*, 2019, **6**, 461401, DOI: **10.3389/fcvm.2019.00089**.

62 A. Badran, *et al.*, Reactive Oxygen Species: Modulators of Phenotypic Switch of Vascular Smooth Muscle Cells, *Int. J. Mol. Sci.*, 2020, **21**(22), 8764, DOI: **10.3390/ijms21228764**.

63 R. H. Burdon, Control of cell proliferation by reactive oxygen species, *Biochem. Soc. Trans.*, 1996, **24**(4), 1028, DOI: **10.1042/bst0241028**.

64 M. Travnickova, *et al.*, Titanium-Doped Diamond-like Carbon Layers as a Promising Coating for Joint Replacements Supporting Osteogenic Differentiation of Mesenchymal Stem Cells, *Int. J. Mol. Sci.*, 2024, **25**(5), 2837, DOI: **10.3390/ijms25052837**.

65 M. L. Circu, *et al.*, Glutathione and modulation of cell apoptosis, *Biochim. Biophys. Acta, Mol. Cell Res.*, 2012, **1823**(10), 1767, DOI: **10.1016/j.bbamcr.2012.06.019**.

66 X. Wu, *et al.*, Citric acid modification of a polymer exhibits antioxidant and anti-inflammatory properties in stem cells

and tissues, *J. Biomed. Mater. Res., Part A*, 2019, **107**(11), 2414, DOI: **10.1002/jbm.a.36748**.

67 A. J. Cumpata, *et al.*, Towards Regenerative Audiology: Immune Modulation of Adipose-Derived Mesenchymal Cells Preconditioned with Citric Acid-Coated Antioxidant-Functionalized Magnetic Nanoparticles, *Medicina*, 2023, **59**(3), 587, DOI: **10.3390/medicina59030587**.

68 C. Kaya, *et al.*, Citric acid and hydrogen sulfide cooperate to mitigate chromium stress in tomato plants by modulating the ascorbate-glutathione cycle, chromium sequestration, and subcellular allocation of chromium, *Environ. Pollut.*, 2023, **335**, 122292, DOI: **10.1016/j.envpol.2023.122292**.

69 M. Weber, *et al.*, Blood-Contacting Biomaterials: In Vitro Evaluation of the Hemocompatibility, *Front. Bioeng. Biotechnol.*, 2018, **6**, 395774, DOI: **10.3389/fbioe.2018.00099**.

70 W. Eggert-Kruse, *et al.*, Clinical relevance of polymorphonuclear (PMN-) elastase determination in semen and serum during infertility investigation, *Int. J. Androl.*, 2009, **32**(4), 317, DOI: **10.1111/j.1365-2605.2007.00852.x**.

71 N. P. Rhodes, *et al.*, Plasma recalcification as a measure of contact phase activation and heparinization efficacy after contact with biomaterials, *Biomaterials*, 1994, **15**(1), 35, DOI: **10.1016/0142-9612(94)90194-5**.

72 H. J. Wedner, *et al.*, Inhibition of human polymorphonuclear leukocyte function by 2-cyclohexene-1-one. A role for glutathione in cell activation, *J. Clin. Invest.*, 1981, **68**(2), 535, DOI: **10.1172/JCI110285**.

73 A. Abnousian, *et al.*, Glutathione Modulates Efficacious Changes in the Immune Response against Tuberculosis, *Biomedicines*, 2023, **11**(5), 1340, DOI: **10.3390/biomedicines11051340**.

74 X. Guan, *et al.*, A general protocol for temperature calibration of MAS NMR probes at arbitrary spinning speeds, *Solid State Nucl. Magn. Reson.*, 2010, **38**(2–3), 74, DOI: **10.1016/j.ssnmr.2010.10.001**.